Matter and Radiation at Extremes REVIEW scitation.org/journal/mre

Dielectronic recombination in non-LTE plasmas

Cite as: Matter Radiat. Extremes 5, 064201 (2020); doi: 10.1063/5.0014158
Submitted: 18 May 2020 • Accepted: 2 September 2020 •
Published Online: 5 October 2020

F. B. Rosmej,[1,2,3,4,a)] V. A. Astapenko,[3] V. S. Lisitsa,[3,4,5] and L. A. Vainshtein[6]

AFFILIATIONS

[1]Sorbonne University, Faculty of Science and Engineering, UMR 7605, Case 128, 4 Place Jussieu, F-75252 Paris Cedex 05, France
[2]LULI, Ecole Polytechnique, CNRS-CEA, Physique Atomique dans les Plasmas Denses (PAPD), Route de Saclay, F-91128 Palaiseau Cedex, France
[3]Moscow Institute of Physics and Technology MIPT (National Research University), Dolgoprudnyi 141700, Russia
[4]National Research Nuclear University—MEPhI, Department of Plasma Physics, Moscow 115409, Russia
[5]National Research Center "Kurchatov Institute", Moscow, Russia
[6]P. N. Lebedev Physical Institute of the Russian Academy of Sciences, Moscow 119991, Russia

Note: This paper is part of the Special Issue on Atomic and Molecular Physics for Controlled Fusion and Astrophysics.
[a)]**Author to whom correspondence should be addressed:** frank.rosmej@sorbonne-universite.fr

ABSTRACT

Novel phenomena and methods related to dielectronic capture and dielectronic recombination are studied for non-local thermodynamic equilibrium (LTE) plasmas and for applications to non-LTE ionization balance. It is demonstrated that multichannel autoionization and radiative decay strongly suppress higher-order contributions to the total dielectronic recombination rates, which are overestimated by standard approaches by orders of magnitude. Excited-state coupling of dielectronic capture is shown to be much more important than ground-state contributions, and electron collisional excitation is also identified as a mechanism driving effective dielectronic recombination. A theoretical description of the effect of angular-momentum-changing collisions on dielectronic recombination is developed from an atomic kinetic point of view and is visualized with a simple analytical model. The perturbation of the autoionizing states due to electric fields is discussed with respect to ionization potential depression and perturbation of symmetry properties of autoionization matrix elements. The first steps in the development of statistical methods are presented and are realized in the framework of a local plasma frequency approach. Finally, the impact of collisional–radiative processes and atomic population kinetics on dielectronic recombination is critically discussed, and simple analytical formulas are presented.

I. INTRODUCTION

Atomic populations are of fundamental importance in a variety of areas in both pure and applied science. Examples include the equation of state in thermodynamics; absorption, emission, and scattering processes in matter; lasing; radiation transport; radiative cooling and energy loss; diagnostic and spectroscopic methods that employ the radiative properties of matter; astrophysics and planetary science; the physics of radiation sources; and fusion science and technology.[1,2]

In a plasma, several charge states usually exist simultaneously, and therefore the total radiation emission arises from excited states of different ionic charges. This indicates that not only are the populations of excited states and their excitation mechanisms relevant but so too is the ionization balance. In hot plasmas, while the excited-state populations are essentially driven by electron collisional excitation, the ionization balance depends strongly on ionization and recombination processes. As shown by Burgess[3] in the context of an analysis of solar emission, electron collisional ionization and radiative recombination alone could not account for observations, and dielectronic recombination was proposed to explain a low level of ionization. In considering radiation balance, it is therefore important to take account of dielectronic recombination. Similarly, the concept of local thermodynamic equilibrium (LTE) depends not only on radiative and collisional rates (as in the traditional description), but on autoionization rates too.

Dielectronic recombination (DR) is the capture of an electron with simultaneous excitation of an atomic core and subsequent radiative stabilization of the core. Within the framework of a simplified model, DR can be viewed as a sequence involving dielectronic capture of a continuum electron into the state nl and subsequent radiative stabilization. The first step is the capture of

an electron into the state nl with simultaneous excitation of the atomic core from state α_0 to state α:

$$\text{dielectronic capture}: A^{+Z}(\alpha_0) + e \rightarrow A^{+(Z-1)^{**}}(\alpha nl). \tag{1.1}$$

After dielectronic capture, autoionization or radiative stabilization can take place:

$$\text{autoionization}: A^{+(Z-1)^{**}}(\alpha nl) \rightarrow A^{+Z}(\alpha_0) + e_{\text{Auger}}. \tag{1.2}$$

The radiative stabilization involves the core and the captured electron (spectator electron):

$$\text{core stabilization}: A^{+(Z-1)^{**}}(\alpha nl) \rightarrow A^{+(Z-1)^{*}}(\alpha_0 nl) + \hbar\omega_{\text{core}}, \tag{1.3}$$

$$\text{spectator electron stabilization}: A^{+(Z-1)^{*}}(\alpha_0 nl) \rightarrow A^{+(Z-1)}(\gamma) + \hbar\omega_{nl}. \tag{1.4}$$

Here, $A^{+(Z-1)^{**}}$ denotes a doubly excited state, $A^{+(Z-1)^{*}}$ a singly excited state, and γ the ground state of the ion in charge state $Z-1$, i.e., $A^{+(Z-1)}(\gamma) = A^{+(Z-1)}(\text{ground})$. The radiation emission of the core [the relation (1.3)] is known as dielectronic satellite emission and has properties that are of great importance for plasma temperature diagnostics, as revealed in the pioneering work by Gabriel.[4] The study of dielectronic satellite emission has become a major aspect of the characterization of a variety of complex phenomena in nonequilibrium plasmas: determination of electron density by angular-momentum-changing collisions[2,5–7] and by the Stark effect;[8,9] characterization and measurement of hot electrons and classification of related instabilities;[10–12] determination of Auger electron heating phenomena in X-ray free-electron laser (XFEL) interaction with solid matter;[13] radiation field analysis via hollow ion X-ray emission;[14,15] collisional phenomena induced by laser-produced plasma jets;[16,17] impurity transport and charge-exchange phenomena with the neutral background in magnetic fusion plasmas;[18,19] relaxation phenomena in fluctuating plasmas;[20] disappearance of resonance line emission followed by accumulation of dielectronic satellite emission;[21–24] ionization potential depression analysis via two-dimensional maps of hollow-ion X-ray emission in XFEL–solid matter interaction.[25] It should be noted here that for diagnostic purposes, radiation transport of radiative transitions originating from autoionizing states should be avoided, because re-emission of the photons is considerably reduced owing to the high autoionization rates.[16]

Comparison of the relations (1.1) and (1.4) shows that effective recombination occurs because an ion A^{+Z} is finally transformed into an ion $A^{+(Z-1)}$. As was demonstrated in Refs. 3 and 26, DR can even be the most important recombination process. As a rule, the DR rate is high for ions with a complex core that exhibits transitions between levels without any change in principal quantum number, i.e., transitions with $\Delta n = 0$, such as $2s \rightarrow 2p$ transitions in lithium-like and more complex ions. It is obvious that, particularly for ions with a complex core, the number of angular momentum coupling possibilities for the whole series of captured electrons is enormous. Therefore, the corresponding atomic structure calculations that combine all the single contributions (1.1)–(1.4) to give the total DR of each ion are numerically prohibitive, and this has manifested itself in a continuing controversy regarding the calculation of the ionic fractions.[27–29]

Moreover, the total DR rate is not an issue of atomic structure calculations alone, but also requires consideration of populations that are strongly out of LTE and consideration of the plasma electric microfield. Therefore, the theoretical determination of the total DR in a nonequilibrium plasma cannot be done within the framework of atomic structure calculations alone.

The present paper is therefore devoted to a critical analysis of methods for the determination of the total DR rate and to develop a new framework to address the challenges faced. In this respect, a rather surprising element is discovered that can be illustrated via the above-mentioned $\Delta n = 0$ transitions, e.g., $2s \rightarrow 2p$ transitions in lithium-like and more complex ions. The transition energy $\Delta E = \hbar\omega_{\text{core}}$ for $\Delta n = 0$ and $Z \gg 1$ is of the order of ZRy, while the ionization energy is of the order of $Z^2Ry \gg \Delta E$. The $2s \rightarrow 2p$ transition is the main channel for both the autoionization and radiative decay. Since the energy E of the incident recombining electron is in all cases smaller than the excitation energy, this implies the following inequality [using $Ry = \frac{1}{2}m_e(c\alpha)^2$ and $E = \frac{1}{2}m_e v_e^2$]:

$$\frac{Z^2 Ry}{E} = \left(\frac{Z\,\alpha c}{v_e}\right)^2 \equiv \eta^2 \gg 1, \tag{1.5}$$

where η is the Coulomb parameter (note that the standard Coulomb parameter determines the possibility of a quasiclassical consideration). The condition (1.5) indicates the validity of the quasiclassical regime in which, for example, the spectrum from the quantum theory of bremsstrahlung[30] coincides with the classical spectrum.[31] Thus, an important part of the overall DR processes is described well by a quasiclassical approach. This opens up new ways to treat important phenomena occurring in plasmas other than purely quantum mechanical atomic structure calculations (e.g., the multiconfiguration Dirac–Fock method).

On the other hand, DR related to $\Delta n = 1$ transitions may require quantum mechanical approaches. A typical example is provided by the core transitions $1s \rightarrow 2p$ in H-like, He-like, etc. ions. Here, the $1s \rightarrow 2p$ transition is the main radiation channel, while the autoionization channel depends strongly on the state nl of the captured electron: for large quantum numbers n, we encounter autoionization according to $2pnl \rightarrow 2s + e$, while for small quantum numbers, the autoionization channel $2pnl \rightarrow 1s + e$ is dominant. For the case $1s \rightarrow 2p$, the transition energy $\Delta E = \hbar\omega_{\text{core}}$ is of the order of Z^2Ry and thus of the same order as the ionization energy. Therefore, the Coulomb parameter is about $\eta \approx 1$ and quantum mechanical calculations might be required.

The paper considers the most recent developments that allow a unique description of the relevant phenomena in DR in nonequilibrium plasmas. For a review of standard methods in the theory of DR, the reader is referred to Refs. 26 and 32–34. In Sec. II, general DR formulas are derived in terms of atomic structure and collisional–radiative decay probabilities. In Sec. III, quantum mechanical multichannel methods are developed and then in Sec. IV, excited-state coupling driven by electron collisional excitation is considered. In Sec. V, the impact of angular-momentum-changing collisions on DR is considered and visualized with a simple analytical approach. Plasma electric field effects are discussed in Sec. VI, where the impacts of ionization potential depression and of symmetry perturbations of autoionizing matrix elements are described. Finally, Sec. VII develops a local plasma frequency statistical approach to calculate DR rates for very complex ions.

II. AUTOIONIZATION, DIELECTRONIC CAPTURE, AND DIELECTRONIC RECOMBINATION

Let us recall the essence of the DR process. An incident electron with energy E excites an ion core with excitation energy $\Delta E = \hbar\omega_{\rm core}$. In this case, if the energy E is smaller than ΔE, the electron is finally captured by the ion into a state with energy $E_f \approx -Ry Z_{\rm eff}^2/n_f^2$ ($Z_{\rm eff}$ is the effective charge of the excited ion core and n_f is the principal quantum number of the captured electron) obeying the condition

$$E - E_f = \Delta E = \hbar\omega_{\rm core} \approx E + Ry\, Z_{\rm eff}^2/n_f^2. \tag{2.1}$$

This capture results in a doubly excited state of the ion; i.e., the ion core electron is excited with energy ΔE, while the captured electron occupies a highly excited level of the ion. This state of the ion can decay in two possible ways:

(i) by relaxation of the ion core electron into the initial ground state with simultaneous ejection of the captured electron from the ion: this process is known as autoionization [compare with the relation (1.2)];
(ii) by radiative decay of the ion core electron, resulting in its return to the initial state after the emission of a photon of energy $\hbar\omega \approx \hbar\omega_{\rm core} = \Delta E$, whereas the captured electron remains bound to the ion [compare with the relation (1.3)].

For illustration, Fig. 1 shows the relevant energy–level diagram for the He-like $2l2l'$ autoionizing levels from which the so-called Ly_α satellites originate. The energy of the $2l2l'$ levels is given approximately by $E_{2l2l'} \approx 2Z_{\rm eff}^2 Ry/4 = Z_{\rm eff}^2 Ry/2$ (in the H-like approximation), which is about half of the ionization energy of the H-like ground state $Z_n^2 Ry$ (where Z_n is the nuclear charge). The series limit of the autoionizing levels $2nl'$ is the first excited state $2l$. Radiative decay (dielectronic satellite emission) from the $2l2l'$ levels populates the singly excited levels $1s2l^{1,3}L$, from which further radiative decays proceed (e.g., the resonance line W = $1s2p\ ^1P_1 - 1s^2\ ^1S_0$ and the intercombination line Y = $1s2p\ ^3P_1 - 1s^2\ ^1S_0$) that finally populate the ground state $1s^2\ ^1S_0$.

The chain of processes of dielectronic capture ($1s + e \to 2l2l'$), radiative decay to singly excited levels ($2l2l' - 1s2l + h\nu$), and radiative decay to the ground state ($1s2l^{1,3}L \to 1s^2\ ^1S_0 + h\nu'$) is called dielectronic recombination (the DR channel) because an effective recombination has taken place from the H-like ground state $1s\ ^2S_{1/2}$ to the He-like ground state $1s^2\ ^1S_0$.

Thus, the DR process as well as the photorecombination (PR) process result in the capture of an incident electron and its simultaneous photon emission. The difference is that the photon is emitted by the ion core electron in the DR process rather than by the incident electron as in the PR process. Note that the relationship between the PR and DR processes is analogous to that between standard bremsstrahlung and polarization bremsstrahlung.[35]

The DR rate can be calculated from the autoionization rate of a given atomic state with the help of the principle of detailed balance. The first step is the application of the principle of detailed balance to dielectronic capture, i.e.,

$$n_j^Z \Gamma_{jk}^{Z,Z+1} = n_k^{Z+1} n_e \langle DC\rangle_{kj}, \tag{2.2}$$

where n_j^Z is the atomic population of the autoionizing state, $\Gamma_{jk}^{Z,Z+1}$ is the autoionization rate from state j to a state k with population

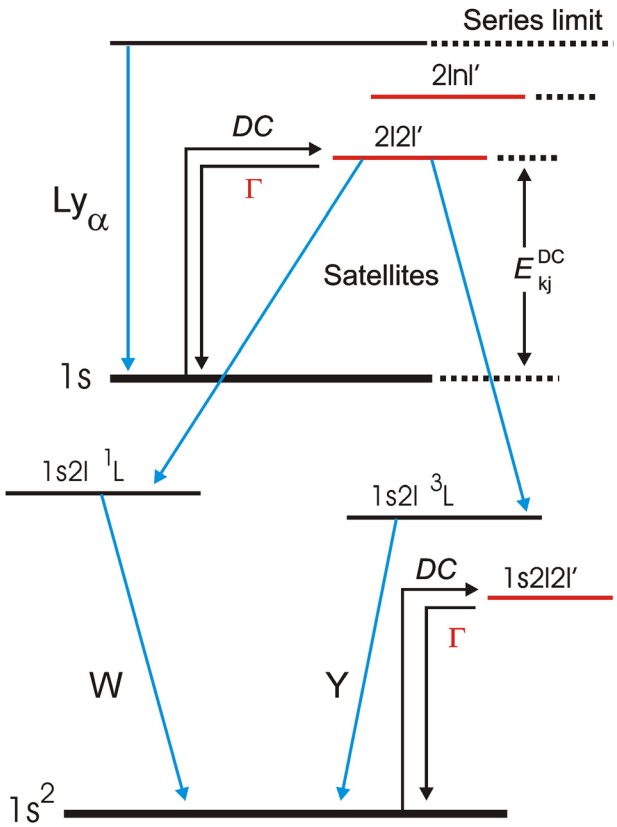

FIG. 1. Energy-level diagram of the He-like autoionizing levels $2l2l'$ and their associated radiative decays, so-called Ly_α satellites. After radiative decay, the singly excited states $1s2l\ ^{1,3}L$ are formed, from which further radiative decay proceeds (e.g., the resonance and intercombination lines W and Y, respectively). Also indicated are the Li-like autoionizing levels $1s2l2l'$.

n_k^{Z+1}, and $\langle DC\rangle_{kj}$ is the dielectronic capture rate from state k to the upper state j. To solve Eq. (2.2) for the dielectronic capture rate, we need to specify the populations. For this purpose, we consider a system in thermodynamic equilibrium. In this case, the populations n_j^Z and n_k^{Z+1} are linked via the Saha–Boltzmann equation, because states j and k belong to different ionic states Z and $Z+1$, respectively, i.e.,

$$\frac{n_j^Z}{n_k^{Z+1}} = n_e \frac{g_j^Z}{2g_k^{Z+1}} \left(\frac{2\pi\hbar^2}{m_e k T_e}\right)^{3/2} \exp\left(\frac{\Delta E_{k,j}^{Z+1,Z}}{kT_e}\right), \tag{2.3}$$

where g_j^Z and g_k^{Z+1} are the statistical weights of states j and k, n_e is the electron density, m_e is the electron mass, and T_e is the electron temperature. The energy difference $\Delta E_{kj}^{Z+1,Z}$ is related to the so-called dielectronic capture energy E_{kj}^{DC} by (see also Fig. 1)

$$\Delta E_{k,j}^{Z+1,Z} = -E_{kj}^{DC}, \tag{2.4}$$

where E_{kj}^{DC} is the energy of the Auger electron if the autoionizing state j decays via autoionization to state k. Combining Eqs. (2.2)–(2.4), we find the general expression for the dielectronic capture rate:

$$\langle DC\rangle_{kj} = \frac{g_j^Z}{2g_k^{Z+1}}\left(\frac{2\pi\hbar^2}{m_e}\right)^{3/2}\Gamma_{jk}^{Z,Z+1}\frac{\exp\left(-E_{kj}^{DC}/kT_e\right)}{(kT_e)^{3/2}}, \tag{2.5}$$

or, in convenient units (with $\Gamma_{jk}^{Z,Z+1}$ in s^{-1}, and E_{kj}^{DC} and T_e in eV),

$$\langle DC\rangle_{kj} = 1.656\times10^{-22}\frac{g_j^Z}{g_k^{Z+1}}\Gamma_{jk}^{Z,Z+1}\frac{\exp\left(-E_{kj}^{DC}/T_e\right)}{T_e^{3/2}}\ (\mathrm{cm}^3/\mathrm{s}) \tag{2.6}$$

[note that Eq. (2.6) assumes a Maxwellian electron energy distribution function with temperature T_e]. If $P_{j,\mathrm{gr}}^Z$ is the probability that the autoionizing state j of charge state Z decays to the ground state of the same charge state, then the quantity $P_{j,\mathrm{gr}}^Z\langle DC\rangle_{kj}$ is called the dielectronic recombination rate coefficient (with units $\mathrm{cm}^3\,\mathrm{s}^{-1}$) into state k via the intermediate state j:

$$\langle DR\rangle_{kj}^{Z+1,Z} = P_{j,\mathrm{gr}}^Z\langle DC\rangle_{kj}^{Z+1,Z}. \tag{2.7}$$

Note that it is important to underline that the assumption of thermodynamic equilibrium to eliminate the populations of Eq. (2.2) with the help of Eq. (2.3) is only a convenient method to apply the principle of detailed balance, but does *not* mean that relations derived with the help of the detailed balance relations are only valid under the assumption of thermodynamic equilibrium. In fact, the dielectronic capture rate [Eq. (2.6)] can also be derived from purely quantum mechanical relations (micro-reversibility), providing a dielectronic capture rate that is also valid for an arbitrary electron energy distribution function $F(E)$:[20]

$$\langle DC\rangle_{kj} = \frac{\pi^2\hbar^3}{\sqrt{2}\,m_e^{3/2}}\frac{g_j^Z}{g_k^{Z+1}}\Gamma_{jk}^{Z,Z+1}\frac{F\left(E_{kj}^{DC}\right)}{\sqrt{E_{kj}^{DC}}}, \tag{2.8}$$

or, in convenient units (with $\Gamma_{jk}^{Z,Z+1}$ in s^{-1}, and $F(E)$, E_{kj}^{DC}, and T_e in eV),

$$\langle DC\rangle_{kj} = 2.9360\times10^{-40}\Gamma_{jk}^{Z,Z+1}\frac{g_j^Z}{g_k^{Z+1}}\Gamma_{jk}^{Z,Z+1}\frac{F\left(E_{kj}^{DC}\right)}{\sqrt{E_{kj}^{DC}}}\ (\mathrm{cm}^3/\mathrm{s}). \tag{2.9}$$

III. TOTAL RATES OF DIELECTRONIC RECOMBINATION: LOW-DENSITY APPROXIMATION

A. General considerations

In general, the probability $P_{j,\mathrm{gr}}^Z$ from Eq. (2.7) is a function of density and temperature, i.e.,

$$P_{j,\mathrm{gr}}^Z = P_{j,\mathrm{gr}}^Z(n_e, T_e). \tag{3.1}$$

The probability function (3.1) has to be determined from numerical calculations of a multilevel multi-charge-state atomic population kinetics that explicitly involves all necessary autoionizing states as "active levels" ("active" here means that the populations of the autoionizing levels are calculated in a similar way to the ground and singly excited states in the population kinetics). If collisions are negligible compared with spontaneous radiative decay rates as well as with autoionization rates, then the probability $P_{j,gr}^Z$ can be approximated by the so-called satellite branching factors B_{ji}^Z:[3]

$$P_{j,\mathrm{gr}}^Z \to \sum_i B_{ji}^Z = \sum_i\left\{\frac{A_{ji}^Z}{\sum_l A_{jl}^Z + \sum_k \Gamma_{jk}^{Z,Z+1}}\right\}. \tag{3.2}$$

That is to say, Eq. (3.2) is the low-density approximation of the probability $P_{j,\mathrm{gr}}^Z$. In this case, the DR rate is given by the following approximate expression:

$$\begin{aligned}\langle DR\rangle_{kj}^{Z+1,Z} &\approx \sum_i B_{ji}^Z.\langle DC\rangle_{kj}^{Z+1,Z}\\ &= \sum_i\left\{\frac{A_{ji}^Z}{\sum_l A_{jl}^Z + \sum_k \Gamma_{jk}^{Z,Z+1}}\langle DC\rangle_{kj}^{Z+1,Z}\right\}.\end{aligned} \tag{3.3}$$

With the help of Eq. (2.5), Eq. (3.3) can be written as follows:

$$\begin{aligned}\langle DR\rangle_{kj}^{Z+1,Z} \approx{}& \frac{1}{2g_k^{Z+1}}\left(\frac{2\pi\hbar^2}{m_e}\right)^{3/2}\\ &\times\frac{\exp\left(-E_{kj}^{DC}/kT_e\right)}{(kT_e)^{3/2}}\sum_i\left\{\frac{g_j^Z\Gamma_{jk}^{Z,Z+1}A_{ji}^Z}{\sum_l A_{jl}^Z + \sum_k \Gamma_{jk}^{Z,Z+1}}\right\}.\end{aligned} \tag{3.4}$$

The term in braces $\{\cdots\}$ is the so-called dielectronic satellite intensity factor

$$Q_{k,ji}^{Z+1,Z} = \frac{g_j^Z\Gamma_{jk}^{Z,Z+1}A_{ji}^Z}{\sum_l A_{jl}^Z + \sum_k \Gamma_{jk}^{Z,Z+1}}, \tag{3.5}$$

which has been calculated by the pioneering work in Refs. 36 and 37 with unprecedented precision via the multiconfiguration Z-expansion method. Therefore, under the assumptions made in Eq. (3.2), the DR rate is given by the sum of the dielectronic satellite intensity factors. One can see that the essential quantities that appear in Eqs. (3.4) and (3.5) to calculate the DR rate in the low-density approximation are the dielectronic capture energy, statistical weights, and radiative and autoionizing decay rates. These quantities can nowadays routinely be generated from atomic structure calculations.

However, as one can see, even for the simplest configurations $2lnl'$, the numerical calculations are rather cumbersome because very large quantum numbers nl' have to be involved to achieve convergence for the DR rates. For large quantum numbers, however, convergence is difficult to achieve in purely quantum numerical atomic structure calculations. Moreover, to obtain the total DR rate from H-like to He-like ions, one needs to invoke all possible intermediate states $j = 3lnl'$, $4lnl'$, $5lnl'$, ...

One can easily understand that for more complex configurations, the number of autoionizing states that need to be involved rapidly becomes numerically prohibitive for purely quantum mechanical numerical calculations. For practical applications, it is therefore mandatory to invoke additional methods, such as the Burgess approach,[3,32] Vainshtein's

simplified quantum mechanical dielectronic recombination model,[26,38] a quasiclassical approach,[31,39] or a statistical approach.[40,41]

B. The Burgess approximation

To illuminate the essence of the various approximations currently employed, we consider first the most general expression for the total dielectronic recombination rate $\langle DR\rangle_{\rm tot}^{Z+1,Z}$. For the total rate, all DR rates $\langle DR\rangle_{kj}^{Z+1,Z} = P_{j,\rm gr}^{Z}\langle DC\rangle_{kj}^{Z+1,Z}$ have to be summed with respect to the initial state k and also with respect to the intermediate states j, i.e.,

$$\langle DR\rangle_{\rm tot}^{Z+1,Z} = \sum_k\sum_j \langle DR\rangle_{kj}^{Z+1,Z} = \sum_k\sum_j P_{j,\rm gr}^{Z}\langle DC\rangle_{kj}^{Z+1,Z}. \quad (3.6)$$

Because the probability $P_{j,\rm gr}^{Z}$ is a function of density and temperature [see Eq. (3.1)], it is very difficult to obtain general and closed formulas for the DR rate coefficient. Only in the low-density approximation, where Eq. (3.3) holds, can general formulas for the DR rate coefficients be obtained.

One of the most widely used general approximate empirical formulas in the framework of the approximation (3.2) is the so-called Burgess formula,[3] in which it is assumed that the nl spectator electron is not interacting with the core and can be treated in the hydrogenic approximation and that the capture cross section averaged over the resonances can be obtained with the aid of the correspondence principle by extrapolating below threshold the partial cross section for the core excitation $\alpha_0 \to \alpha$:

$$\langle DR\rangle_{kj}^{Z+1,Z} := D^{Z+1,Z}(\alpha_0 \to \alpha, nl). \quad (3.7)$$

For the total DR rate, we have

$$\langle DR\rangle_{tot}^{Z+1,Z} := D^{Z+1,Z} = \sum_{\alpha_0}\sum_{\alpha}\sum_{n}\sum_{l=0}^{n-1} D^{Z+1,Z}(\alpha_0 \to \alpha, nl). \quad (3.8)$$

For the simplest example of autoionizing states $2l2l'$ outlined in Fig. 1, $\alpha_0 = 1s$ and $\alpha_1 = 2p$, i.e., the transition $\alpha_0 \to \alpha$ corresponds to the Ly_α transition in H-like ions. For these configurations, DR into the ground state is the most important transition; i.e., there exists a single state $k = \alpha_0 = 1s$. Therefore, α_0 coincides with the atomic ground state, and the sum over α_0 can be suppressed:

$$D^{Z+1,Z} \approx \sum_{\alpha}\sum_{n}\sum_{l=0}^{n-1} D^{Z+1,Z}(\alpha_0 \to \alpha, nl). \quad (3.9)$$

The DR rate coefficient $D^{Z+1,Z}(\alpha_0 \to \alpha, nl)$ can then be expressed via the following analytical empirical expression:[3]

$$D^{Z+1,Z}(\alpha_0 \to \alpha, nl) = 4.8\times10^{-11} f_{\alpha_0\alpha} B_d \beta^{3/2} e^{-\beta\chi_d}\ (\mathrm{cm^3/s}), \quad (3.10)$$

with

$$\beta = \frac{(z+1)^2 Ry}{kT_e}, \quad (3.11)$$

$$\chi_d = \frac{\chi}{1 + 0.015\dfrac{z^3}{(z+1)^2}}, \quad (3.12)$$

$$\chi = \frac{\Delta E(\alpha_0 \to \alpha)}{(z+1)^2 Ry}. \quad (3.13)$$

Here, z is the so-called spectroscopic symbol of the doubly excited ion after recombination, $z = Z_n - N_{\rm bound} + 1$, where $N_{\rm bound}$ is the number of bound electrons and $Z_n e$ is the nuclear charge. If the first resonance transition is a $\Delta n = 0$ transition, then the branching factor B_d is given by the following fitting formula (the so-called Burgess–Mertz formula):[32]

$$B_d = \left(\frac{z\chi}{z^2+13.4}\right)^{1/2} \frac{1}{1 + 0.105(z+1)\chi + 0.015(z+1)^2\chi^2}. \quad (3.14)$$

For $\Delta n \neq 0$ the fitting function for the branching factor B_d is different:[32]

$$B_d = \left(\frac{z\chi}{z^2+13.4}\right)^{1/2} \frac{0.5}{1 + 0.210(z+1)\chi + 0.030(z+1)^2\chi^2}. \quad (3.15)$$

Let us recall the meaning of the branching factor B_d: after dielectronic capture, a doubly excited state is formed that can decay via autoionization or radiative decay. For DR, only the radiative decays contribute finally to recombination, since autoionization returns the autoionizing state to the original state.

According to Eq. (3.10), α_0 is the ground state, and therefore $f_{\alpha 0\alpha}$ is the electric dipole absorption oscillator strength for the resonance transition $\alpha_0 \to \alpha$ with transition energy $\Delta E(\alpha_0 \to \alpha)$ in eV. As the absorption oscillator strength decreases rapidly with increasing principal quantum number of the upper level, it is usually sufficient to consider only the first two α-terms in the sum in Eq. (3.9), and we finally obtain the desired expression for the total DR coefficient:

$$D^{Z+1,Z} \approx D^{Z+1,Z}(\alpha_0 \to \alpha_1) + D^{Z+1,Z}(\alpha_0 \to \alpha_2), \quad (3.16)$$

with

$$D^{Z+1,Z}(\alpha_0 \to \alpha) := \sum_{n}\sum_{l=0}^{n-1} D^{Z+1,Z}(\alpha_0 \to \alpha, nl). \quad (3.17)$$

Let us consider DR into neutral helium as an example (note that a single * indicates a singly excited state, while ** corresponds to a multiply excited state):

$$\mathrm{He}^{1+}(1s) + e \to \mathrm{He}^{0+**}(nln'l') \to \mathrm{He}^{0+}(1s^2). \quad (3.18)$$

For this example, $\alpha_0 = 1s$, $\alpha_1 = 2p$, $\alpha_2 = 3p$, ... Therefore, $f_{\alpha_0\alpha_1}$ corresponds to the electric dipole absorption oscillator strength of the resonance line, namely, the H-like Ly_α line of singly ionized helium, while $f_{\alpha_0\alpha_2}$ corresponds to the Ly_β line. The oscillator strengths are $f_{1s\to2p} = 0.4164$ and $f_{1s\to3p} = 0.079\,14$, and their transition energies are $\Delta E(1s \to 2p) = 40.81$ eV and $\Delta E(1s \to 3p) = 48.37$ eV. The spectroscopic symbol is $z = 1$ and $\Delta n \neq 0$ [therefore, Eq. (3.15) applies]. As one can see, higher-n oscillator strengths make almost negligible contributions to the total DR rate (note that this has to be

distinguished from the fact that high-n spectator electrons can make quite important contributions). From Eqs. (3.11)–(3.13), we obtain $\beta = 4\mathrm{Ry}/kT_e$, $B_d(1s \to 2p) = 0.0825$, $B_d(1s \to 3p) = 0.0846$, $\chi_d(1s \to 2p) = 0.747$, and $\chi_d(1s \to 3p) = 0.886$. For the rate coefficients at $kT_e = Ry$ ($\beta = 4$), we obtain $D^{He^{1+},He^{0+}}(1s \to 2p) = 1.65 \times 10^{-12}$ cm^3/s, and $D^{He^{1+},He^{0+}}(1s \to 3p) = 3.2 \times 10^{-13}$ cm^3/s. This confirms that the leading terms for DR are indeed given by Eq. (3.16).

C. Quantum mechanical multichannel approach

Comparison of the results from Eqs. (3.10)–(3.15) with more precise quantum mechanical calculations carried out with Vainshtein's ATOM code[42,43] show that the χ_d values are in quite good agreement, whereas the B_d values differ strongly. For the resonance transitions $1s \to 2p$ and $1s \to 3p$, the B_d values obtained from Vainshtein's simplified quantum mechanical multi-channel (QMMC) approach[38,44] for the above example of helium are significantly different, namely, $B_{d,\mathrm{ref}}(1s \to 2p) = 0.155$, $B_{d,\mathrm{ref}}(1s \to 3p) = 0.0144$, $\chi_{d,\mathrm{ref}}(1s \to 2p) = 0.744$, and $\chi_{d,\mathrm{ref}}(1s \to 3p) = 0.888$, giving $D_{\mathrm{ref}}^{He^{1+},He^{0+}}(1s \to 2p) = 3.10 \times 10^{-12}$ cm^3/s and $D_{\mathrm{ref}}^{He^{1+},He^{0+}}(1s \to 3p) = 5.46 \times 10^{-14}$ cm^3/s, i.e., the Burgess formula underestimates the B_d value for $\alpha_0 \to \alpha = 1s \to 2p$ by a factor of 2 and overestimates the B_d value for $\alpha_0 \to \alpha = 1s \to 3p$ by a factor of 6. These are general observations: the precision of Eqs. (3.10)–(3.15) is very difficult to estimate: it might be about a factor of 2 for the strongest resonance transition, but it might also deviate by orders of magnitude.

Understanding the large overestimate of the B_d value for the transition $1s \to 3p$ is of particular importance and is related to the fact that the Burgess formulas take into account only one autoionizing channel. For example, the $3lnl'$-configurations (which are related to the transition $\alpha_0 \to \alpha_2 = 1s \to 3p$ in the above example) autoionize not only to the ground state but to excited states too:

$$3lnl' \to \left\{ \begin{array}{l} 1s + e_{\mathrm{Auger}} \\ 2l + e_{\mathrm{Auger}} \end{array} \right\}. \tag{3.19}$$

Complex numerical multiconfiguration Hartree–Fock calculations show[23,45] that the autoionization rates to the excited states "$2l$" are even more important than to the ground state "$1s$." This reduces considerably the branching factor for DR [the B_d factor in Eq. (3.10)]. In fact, as one can see from Eq. (3.15), very similar branching factors are given for the transitions $\alpha_0 \to \alpha_1 = 1s \to 2p$ and $\alpha_0 \to \alpha_2 = 1s \to 3p$ because only one autoionizing channel is taken into consideration.

It is very important for the practical application of DR rates in the modeling of ionization balance to explore in more detail the influence of the various multiple channels for Auger and radiative decay. Below, we perform QMMC calculations for DR in the simplified Vainshtein approach,[38,42–44] and we fit the numerical results to an analytical expression in order to facilitate the application and allow direct comparison with the Burgess formulas:

$$D^{Z+1,Z}(\alpha_0 \to \alpha, nl) = 10^{-8} \times \frac{m}{2l_0 + 1} B_d \beta^{3/2} e^{-\beta\chi_d} \ (\mathrm{cm}^3/\mathrm{s}), \tag{3.20}$$

$$\beta = \frac{Z^2\, Ry}{kT_e}, \tag{3.21}$$

where $Ry = 13.6057$ eV, kT_e is the electron temperature in eV, m is the number of equivalent electrons of state α_0, Z is the charge of the ion where the core transition $\alpha_0 \to \alpha$ takes place (e.g., for the $2lnl'$ autoionizing states of He-like argon, the core transition is the $1s \to 2p$ transition in H-like argon, $Z = 18$), and l_0 is the corresponding orbital momentum of state α_0. The physical meaning of the parameter χ_d is related to the fact that all contributions from the configurations with different spectator electrons nl have to be summed up to give the total DR rate with different energies [see Eq. (2.1)]. The parameter χ_d provides a fit to the numerical results to replace the sum of different energies in the best manner through an average energy parameter $\chi_d\beta$. Finally, the total sum is replaced by an average amplitude B_d to provide a simple analytical expression without the need for summation.

As a demonstration, let us consider the various mechanisms via a study of the DR related to the core transition $2s$–$4p$. For example, the numerical calculations in the single-channel approximation for Be atoms give $B_d^{(1-\mathrm{channel})}(2s-3p) = 3.4 \times 10^{-5}$, whereas $B_d^{(1-\mathrm{channel})}(2s-4p) = 1.6 \times 10^{-5}$; i.e., $2s$–$4p$ transitions are only reduced by a factor of about two compared with $2s$–$3p$ transitions. Numerical calculations including multichannel decay provide an entirely different picture, with $B_d^{(6-\mathrm{channel})}(2s-3p) = 2.0 \times 10^{-6}$, but $B_d^{(6-\mathrm{channel})}(2s-4p) = 3.5 \times 10^{-7}$; i.e., the QMMC numerical calculations indicate that higher-order DR rates are strongly suppressed. This is a general observation that multichannel decay can reduce DR considerably and can even lead to a quite different interpretation of its importance.

Table I shows the numerical calculation for the DR B_d factors for single- and multichannel decay into Li-like ions for different orders and elements in comparison with the standard Burgess formula. One observes that the Burgess formula is in reasonable agreement with the numerical results for single-channel decay, although it differs by up to a factor of 3 in some cases. However, comparison with the numerical calculations using the QMMC approach reveals extremely large overestimates of DR obtained by the Burgess formula. In particular for light elements, the overestimation can be by as much as one or two orders of magnitude: for example, for the DR related to the autoionizing states $1s^2 4lnl'$ of Be, we have $B_d^{(\mathrm{multichannel})}(2s-4p) = 3.47 \times 10^{-7}$ and $B_d^{(\mathrm{Burgess})}(2s-4p) = 1.10 \times 10^{-5}$; i.e., the Burgess formula overestimates B_d by more than a factor of 30. It is therefore *not* recommended to calculate higher-order contributions to DR via the Burgess approach.

In Tables II–IV, we present the numerical results of the QMMC approach for H-, He-, and Li-like ions, which are the most important for K-shell spectroscopy. For ease of application, we have fitted all results to the simple analytical formula (3.20).

Table II presents the results of a numerical calculation of the total DR rate into H-like ions for the core transitions $1s$–$2p$ and $1s$–$3p$ for all elements from He ($Z = 2$) up to Mo ($Z = 42$) and the corresponding fitting parameters according to Eq. (3.20). It can be seen that for low-Z elements, the DR related to the core transition $1s$–$2p$ is dominant, whereas for large Z, the relative contribution of the DR with the core transition $1s$–$3p$ increases. The Burgess formula provides amplitudes B_d that are about a factor of 3 smaller than the present numerical calculations.

TABLE I. B_d factors according to Eqs. (3.20) and (3.21) for DR into Li-like ions originating from the $1s^2nln'l'$ autoionizing levels, with $Z = Z_n - 2$, $m = 1$, and $l_0 = 0$. The numerical data show single- and multichannel approximations as well as the corresponding factors according to the Burgess approach (note that the different numerical coefficients and the oscillator strength in the original Burgess formula [Eq. (3.10)] compared with Eq. (3.20) have been included in the value for $B_d^{(\mathrm{Burgess})}$ to facilitate comparison of the different methods).

Element	$B_d^{(1-\mathrm{channel})}$	$B_d^{(\mathrm{multichannel})}$	$B_d^{(\mathrm{Burgess})}$
	$1s^22lnl'$: $\alpha_0 = 1s^22s \rightarrow \alpha = 1s^22p$		
Be	8.09×10^{-5}	...	1.34×10^{-4}
C	5.18×10^{-5}	...	7.99×10^{-5}
Mg	1.34×10^{-5}	...	1.94×10^{-5}
Ar	6.87×10^{-6}	...	8.65×10^{-6}
Fe	4.02×10^{-6}	...	4.88×10^{-6}
Mo	3.11×10^{-6}	...	3.87×10^{-6}
	$1s^23lnl'$: $\alpha_0 = 1s^22s \rightarrow \alpha = 1s^23p$		
Be	3.44×10^{-5}	1.97×10^{-6}	2.88×10^{-5}
C	6.45×10^{-5}	6.61×10^{-6}	6.98×10^{-5}
Mg	6.43×10^{-5}	2.57×10^{-5}	6.96×10^{-5}
Ar	4.55×10^{-5}	2.42×10^{-5}	5.15×10^{-5}
Fe	2.61×10^{-5}	1.57×10^{-5}	3.54×10^{-5}
Mo	8.61×10^{-6}	6.48×10^{-6}	1.89×10^{-5}
	$1s^24lnl'$: $\alpha_0 = 1s^22s \rightarrow \alpha = 1s^24p$		
Be	1.60×10^{-5}	3.47×10^{-7}	1.10×10^{-5}
C	2.52×10^{-5}	3.39×10^{-7}	2.23×10^{-5}
Mg	2.06×10^{-5}	1.30×10^{-6}	1.87×10^{-5}
Ar	1.29×10^{-5}	2.05×10^{-6}	1.27×10^{-5}
Fe	6.54×10^{-6}	2.00×10^{-6}	8.01×10^{-6}
Mo	1.87×10^{-6}	1.17×10^{-6}	3.82×10^{-6}

For the $3lnl'$ states, the Burgess formula considerably overestimates the DR rate because it does not take into account multichannel radiative and Auger decays. This is of particular importance for low-Z elements. For example, for C, the single-channel approximation gives $B_d = 6.75 \times 10^{-5}$, whereas the four-channel approximation gives $B_d = 6.32 \times 10^{-6}$, i.e., a reduction by a factor of 10. Multichannel decay is much less important for higher Z: for example, for Fe, $B_d = 5.13 \times 10^{-6}$, whereas the four-channel approximation gives $B_d = 2.60 \times 10^{-6}$.

Table III presents numerical results for the total DR rate into He-like ions for the core transitions $1s$–$2p$ and $1s$–$3p$ for all elements from He ($Z = 2$) up to Mo ($Z = 42$) and the corresponding fitting parameters according to Eq. (3.20). It can be seen that for low-Z elements, the DR related to the core transition $1s$–$2p$ is dominant, whereas for large Z, the relative contribution of the DR with the core transition $1s$–$3p$ increases. The Burgess formula gives amplitudes B_d that are about a factor of 3 smaller than the present numerical calculations. For the $1s3lnl'$ states, the Burgess formula considerably overestimates the DR rate because it does not take into account multichannel radiative and Auger decays. This is of particular importance for low-Z elements. For example, for C, the single-channel approximation gives $B_d = 6.76 \times 10^{-5}$, whereas the four-channel approximation gives $B_d = 2.98 \times 10^{-6}$, i.e., a reduction by a factor of 20. Multichannel decay is much less important for higher Z: for example, for Fe, $B_d = 5.34 \times 10^{-6}$, whereas the four-channel approximation gives $B_d = 2.60 \times 10^{-6}$.

TABLE II. Fitting coefficients according to Eqs. (3.20) and (3.21) for DR into H-like ions originating from the 2lnl′ and 3lnl′ autoionizing levels, with $Z = Z_n$, $m = 1$, and $l_0 = 0$. The numerical data include corrections for multiple decay channels (two channels for $2lnl'$ and four channels for 3lnl′).

	$2lnl'$: $\alpha_0 = 1s \rightarrow \alpha = 2p$		$3lnl'$: $\alpha_0 = 1s \rightarrow \alpha = 3p$	
Element	B_d	χ_d	B_d	χ_d
He	3.12×10^{-4}	0.744	5.48×10^{-6}	0.888
Li	3.72×10^{-4}	0.736	6.41×10^{-6}	0.887
Be	3.67×10^{-4}	0.727	6.53×10^{-6}	0.885
B	3.42×10^{-4}	0.718	6.47×10^{-6}	0.883
C	3.13×10^{-4}	0.709	6.32×10^{-6}	0.881
N	2.85×10^{-4}	0.700	6.31×10^{-6}	0.879
O	2.58×10^{-4}	0.691	5.92×10^{-6}	0.877
F	2.33×10^{-4}	0.682	5.70×10^{-6}	0.874
Ne	2.11×10^{-4}	0.673	5.48×10^{-6}	0.872
Na	1.90×10^{-4}	0.665	5.26×10^{-6}	0.870
Mg	1.72×10^{-4}	0.657	5.04×10^{-6}	0.868
Al	1.56×10^{-4}	0.649	4.84×10^{-6}	0.866
Si	1.41×10^{-4}	0.642	4.63×10^{-6}	0.863
P	1.27×10^{-4}	0.636	4.43×10^{-6}	0.861
S	1.15×10^{-4}	0.630	4.24×10^{-6}	0.859
Cl	1.05×10^{-4}	0.624	4.05×10^{-6}	0.857
Ar	9.50×10^{-5}	0.620	3.87×10^{-6}	0.856
K	8.61×10^{-5}	0.616	3.69×10^{-6}	0.854
C	7.82×10^{-5}	0.612	3.52×10^{-6}	0.852
Sc	7.09×10^{-5}	0.609	3.35×10^{-6}	0.851
Ti	6.45×10^{-5}	0.606	3.19×10^{-6}	0.849
V	5.85×10^{-5}	0.604	3.04×10^{-6}	0.848
Cr	5.33×10^{-5}	0.602	2.89×10^{-6}	0.847
Mn	4.85×10^{-5}	0.601	2.74×10^{-6}	0.846
Fe	4.42×10^{-5}	0.599	2.60×10^{-6}	0.845
Co	4.03×10^{-5}	0.598	2.47×10^{-6}	0.844
Ni	3.68×10^{-5}	0.598	2.34×10^{-6}	0.843
Cu	3.37×10^{-5}	0.597	2.22×10^{-6}	0.842
Zn	3.08×10^{-5}	0.597	2.10×10^{-6}	0.842
Ga	2.83×10^{-5}	0.596	1.99×10^{-6}	0.842
Ge	2.60×10^{-5}	0.596	1.88×10^{-6}	0.841
As	2.39×10^{-5}	0.596	1.78×10^{-6}	0.841
Se	2.20×10^{-5}	0.596	1.68×10^{-6}	0.841
Br	2.03×10^{-5}	0.596	1.59×10^{-6}	0.841
Kr	1.88×10^{-5}	0.596	1.50×10^{-6}	0.841
Rb	1.74×10^{-5}	0.597	1.42×10^{-6}	0.841
Sr	1.61×10^{-5}	0.597	1.34×10^{-6}	0.842
Y	1.50×10^{-5}	0.597	1.27×10^{-6}	0.842
Zr	1.39×10^{-5}	0.598	1.20×10^{-6}	0.842
Nb	1.30×10^{-5}	0.599	1.13×10^{-6}	0.843
Mo	1.21×10^{-5}	0.599	1.07×10^{-6}	0.843

Table IV presents numerical results for DR into Li-like ions related to the core transition $2s$–$2p$, i.e., a $\Delta n = 0$ transition. Therefore, the fitting parameter χ_d is rather small and the associated exponential factor for DR does not vary much. In addition, the configurations $1s^22lnl'$ are only autoionizing for rather high principal quantum

TABLE III. Fitting coefficients according to Eqs. (3.20) and (3.21) for DR into He-like ions originating from the $1s2lnl'$ and $1s3lnl'$ autoionizing levels, with $Z = Z_n - 1$, $m = 2$, and $l_0 = 0$. The numerical data include corrections for multiple decay channels (two channels for $1s2lnl'$ and four channels for $1s3lnl'$).

	$1s2lnl'$: $\alpha_0 = 1s^2 \rightarrow \alpha = 1s2p$		$1s3lnl'$: $\alpha_0 = 1s^2 \rightarrow \alpha = 1s3p$	
Element	B_d	χ_d	B_d	χ_d
Li	3.39×10^{-5}	1.11	1.57×10^{-6}	1.27
Be	9.94×10^{-5}	0.961	2.12×10^{-6}	1.14
B	1.53×10^{-4}	0.891	2.51×10^{-6}	1.07
C	1.93×10^{-4}	0.848	2.98×10^{-6}	1.03
N	2.17×10^{-4}	0.818	3.40×10^{-6}	1.00
O	2.34×10^{-4}	0.795	3.92×10^{-6}	0.983
F	2.17×10^{-4}	0.775	4.23×10^{-6}	0.967
Ne	2.05×10^{-4}	0.757	4.50×10^{-6}	0.956
Na	1.88×10^{-4}	0.740	4.56×10^{-6}	0.945
Mg	1.72×10^{-4}	0.726	4.54×10^{-6}	0.937
Al	1.57×10^{-4}	0.713	4.47×10^{-6}	0.929
Si	1.43×10^{-4}	0.701	4.36×10^{-6}	0.922
P	1.30×10^{-4}	0.690	4.22×10^{-6}	0.916
S	1.18×10^{-4}	0.681	4.07×10^{-6}	0.910
Cl	1.07×10^{-4}	0.672	3.92×10^{-6}	0.905
Ar	9.72×10^{-5}	0.664	3.76×10^{-6}	0.901
K	8.83×10^{-5}	0.658	3.61×10^{-6}	0.897
C	8.02×10^{-5}	0.652	3.45×10^{-6}	0.893
Sc	7.28×10^{-5}	0.647	3.30×10^{-6}	0.889
Ti	6.62×10^{-5}	0.642	3.15×10^{-6}	0.886
V	6.02×10^{-5}	0.638	3.01×10^{-6}	0.883
Cr	5.47×10^{-5}	0.635	2.87×10^{-6}	0.880
Mn	4.98×10^{-5}	0.632	2.73×10^{-6}	0.877
Fe	4.54×10^{-5}	0.629	2.60×10^{-6}	0.875
Co	4.14×10^{-5}	0.627	2.47×10^{-6}	0.873
Ni	3.78×10^{-5}	0.625	2.35×10^{-6}	0.871
Cu	3.46×10^{-5}	0.623	2.23×10^{-6}	0.869
Zn	3.16×10^{-5}	0.622	2.11×10^{-6}	0.868
Ga	2.90×10^{-5}	0.620	2.00×10^{-6}	0.867
Ge	2.67×10^{-5}	0.619	1.90×10^{-6}	0.865
As	2.45×10^{-5}	0.619	1.80×10^{-6}	0.864
Se	2.26×10^{-5}	0.618	1.70×10^{-6}	0.864
Br	2.08×10^{-5}	0.617	1.61×10^{-6}	0.863
Kr	1.93×10^{-5}	0.617	1.52×10^{-6}	0.862
Rb	1.78×10^{-5}	0.616	1.44×10^{-6}	0.862
Sr	1.65×10^{-5}	0.616	1.36×10^{-6}	0.861
Y	1.53×10^{-5}	0.616	1.29×10^{-6}	0.861
Zr	1.43×10^{-5}	0.616	1.22×10^{-6}	0.861
Nb	1.33×10^{-5}	0.616	1.15×10^{-6}	0.861
Mo	1.24×10^{-5}	0.616	1.09×10^{-6}	0.861

numbers. This is quite different to the DR related to the core transition $2s$–$3p$, where the states are autoionizing for rather low quantum numbers nl and the temperature dependence is very different owing to an order-of-magnitude difference in the χ_d factor.

Unlike DR into H- and He-like ions (Tables II and III), the DR related to the $n = 3$ core transition is very important compared with the $2s$–$2p$ related recombination. For this reason, the temperature dependence of the total recombination rate (which is the sum of the DR rates related to the $2s$–$2p$, $2s$–$3p$, . . ., core transitions) is complex and differs qualitatively from the rates of DR into H- and He-like ions, which are dominated by a single exponential factor.

TABLE IV. Fitting coefficients according to Eqs. (3.20) and (3.21) for DR into Li-like ions originating from the $1s^22lnl'$ and $1s^23lnl'$ autoionizing levels, with $Z = Z_n - 2$, $m = 1$, and $l_0 = 0$. The numerical data include corrections for multiple decay channels (one channel for $1s^22lnl'$ and four channels for $1s^23lnl'$).

	$1s^22lnl'$: $\alpha_0 = 1s^22s \rightarrow \alpha = 1s^22p$		$1s^23lnl'$: $\alpha_0 = 1s^22s \rightarrow \alpha = 1s^23p$	
Element	B_d	χ_d	B_d	χ_d
Be	8.09×10^{-5}	0.057 1	1.97×10^{-6}	0.197
B	6.86×10^{-5}	0.040 0	2.85×10^{-6}	0.173
C	5.18×10^{-5}	0.030 6	6.61×10^{-6}	0.161
N	3.95×10^{-5}	0.024 8	1.06×10^{-5}	0.153
O	3.09×10^{-5}	0.020 7	1.47×10^{-5}	0.149
F	2.47×10^{-5}	0.017 9	1.85×10^{-5}	0.145
Ne	2.02×10^{-5}	0.015 6	2.17×10^{-5}	0.142
Na	1.69×10^{-5}	0.013 9	2.41×10^{-5}	0.140
Mg	1.43×10^{-5}	0.012 6	2.57×10^{-5}	0.138
Al	1.23×10^{-5}	0.011 5	2.67×10^{-5}	0.136
Si	1.07×10^{-5}	0.010 5	2.71×10^{-5}	0.135
P	9.43×10^{-6}	0.009 81	2.69×10^{-5}	0.133
S	8.41×10^{-6}	0.009 14	2.60×10^{-5}	0.131
Cl	7.57×10^{-6}	0.008 58	2.53×10^{-5}	0.130
Ar	6.87×10^{-6}	0.008 09	2.42×10^{-5}	0.128
K	6.25×10^{-6}	0.007 72	2.31×10^{-5}	0.127
C	5.76×10^{-6}	0.007 36	2.19×10^{-5}	0.126
Sc	5.35×10^{-6}	0.007 04	2.09×10^{-5}	0.124
Ti	5.00×10^{-6}	0.006 77	1.97×10^{-5}	0.123
V	4.67×10^{-6}	0.006 58	1.86×10^{-5}	0.122
Cr	4.42×10^{-6}	0.006 37	1.76×10^{-5}	0.120
Mn	4.20×10^{-6}	0.006 20	1.66×10^{-5}	0.119
Fe	4.02×10^{-6}	0.006 05	1.57×10^{-5}	0.118
Co	3.86×10^{-6}	0.005 92	1.48×10^{-5}	0.117
Ni	3.72×10^{-6}	0.005 81	1.40×10^{-5}	0.116
Cu	3.61×10^{-6}	0.005 71	1.32×10^{-5}	0.115
Zn	3.51×10^{-6}	0.005 64	1.25×10^{-5}	0.114
Ga	3.42×10^{-6}	0.005 58	1.18×10^{-5}	0.113
Ge	3.35×10^{-6}	0.005 53	1.11×10^{-5}	0.112
As	3.25×10^{-6}	0.005 56	1.05×10^{-5}	0.111
Se	3.20×10^{-6}	0.005 54	9.96×10^{-6}	0.110
Br	3.20×10^{-6}	0.005 46	9.43×10^{-6}	0.109
Kr	3.17×10^{-6}	0.005 46	8.92×10^{-6}	0.108
Rb	3.15×10^{-6}	0.005 47	8.45×10^{-6}	0.107
Sr	3.13×10^{-6}	0.005 48	8.01×10^{-6}	0.106
Y	3.12×10^{-6}	0.005 51	7.59×10^{-6}	0.105
Zr	3.11×10^{-6}	0.005 54	7.20×10^{-6}	0.105
Nb	3.11×10^{-6}	0.005 58	6.83×10^{-6}	0.104
Mo	3.11×10^{-6}	0.005 63	6.48×10^{-6}	0.103

IV. EXCITED-STATE COUPLING OF DIELECTRONIC RECOMBINATION IN DENSE PLASMAS

Table V shows the DR rates related to the excited states $1s^22p$ of Li-like ions. It can be seen from a comparison of the numerical data in

TABLE V. Fitting coefficients according to Eqs. (3.20) and (3.21) for DR into excited states of Li-like ions originating from the $1s^2 3lnl'$ and $1s^2 4lnl'$ autoionizing levels, with $Z = Z_n - 2$, $m = 1$, and $l_0 = 1$. The numerical data include corrections for multiple decay channels (three channels for $1s^2 3lnl'$ and six channels for $1s^2 4lnl'$).

	$1s^2 3lnl'$: $\alpha_0 = 1s^2 2p \rightarrow \alpha = 1s^2 3d$		$1s^2 4lnl'$: $\alpha_0 = 1s^2 2p \rightarrow \alpha = 1s^2 4d$	
Element	B_d	χ_d	B_d	χ_d
Be	1.78×10^{-4}	0.140	1.88×10^{-5}	0.190
B	2.99×10^{-4}	0.137	2.01×10^{-5}	0.189
C	3.74×10^{-4}	0.135	2.04×10^{-5}	0.188
N	4.44×10^{-4}	0.133	2.18×10^{-5}	0.187
O	5.15×10^{-4}	0.131	2.35×10^{-5}	0.187
F	5.52×10^{-4}	0.130	2.53×10^{-5}	0.186
Ne	5.65×10^{-4}	0.128	2.67×10^{-5}	0.185
Na	5.76×10^{-4}	0.127	2.88×10^{-5}	0.181
Mg	5.73×10^{-4}	0.125	3.28×10^{-5}	0.174
Al	5.61×10^{-4}	0.124	3.32×10^{-5}	0.172
Si	5.39×10^{-4}	0.122	3.33×10^{-5}	0.171
P	5.19×10^{-4}	0.120	3.48×10^{-5}	0.167
S	4.96×10^{-4}	0.119	3.46×10^{-5}	0.165
Cl	4.71×10^{-4}	0.117	3.44×10^{-5}	0.164
Ar	4.48×10^{-4}	0.115	3.41×10^{-5}	0.163
K	4.25×10^{-4}	0.114	3.38×10^{-5}	0.161
C	4.04×10^{-4}	0.112	3.34×10^{-5}	0.160
Sc	3.83×10^{-4}	0.110	3.30×10^{-5}	0.159
Ti	3.64×10^{-4}	0.109	3.25×10^{-5}	0.158
V	3.45×10^{-4}	0.107	3.20×10^{-5}	0.157
Cr	3.27×10^{-4}	0.105	3.14×10^{-5}	0.156
Mn	3.11×10^{-4}	0.104	3.08×10^{-5}	0.156
Fe	2.95×10^{-4}	0.102	3.02×10^{-5}	0.155
Co	2.80×10^{-4}	0.101	2.95×10^{-5}	0.154
Ni	2.66×10^{-4}	0.0992	2.88×10^{-5}	0.154
Cu	2.53×10^{-4}	0.0978	2.80×10^{-5}	0.153
Zn	2.40×10^{-4}	0.0964	2.72×10^{-5}	0.153
Ga	2.28×10^{-4}	0.0951	2.64×10^{-5}	0.153
Ge	2.17×10^{-4}	0.0939	2.56×10^{-5}	0.152
As	2.06×10^{-4}	0.0927	2.47×10^{-5}	0.152
Se	1.96×10^{-4}	0.0916	2.39×10^{-5}	0.152
Br	1.86×10^{-4}	0.0905	2.30×10^{-5}	0.152
Kr	1.77×10^{-4}	0.0895	2.22×10^{-5}	0.152
Rb	1.68×10^{-4}	0.0885	2.14×10^{-5}	0.152
Sr	1.60×10^{-4}	0.0876	2.05×10^{-5}	0.152
Y	1.52×10^{-4}	0.0867	1.97×10^{-5}	0.152
Zr	1.45×10^{-4}	0.0859	1.89×10^{-5}	0.152
Nb	1.38×10^{-4}	0.0851	1.82×10^{-5}	0.152
Mo	1.31×10^{-4}	0.0844	1.74×10^{-5}	0.152

Tables IV and V that the contribution from the excited states is even more important than that from the ground state. For example, for Be, $B_d(2s - 3p) = 1.97 \times 10^{-6}$, whereas $B_d(2p - 3d) = 1.78 \times 10^{-4}$ and $B_d(2p - 4d) = 1.88 \times 10^{-5}$. This means that the excited-state contribution is up to two orders of magnitude larger than the ground-state contribution. Therefore, even for rather moderate densities with small populations of the excited states, their contribution to DR can be important.

Particular important cases are encountered if the first excited states are related to $\Delta n = 0$ radiative transitions. Because these transition probabilities are orders of magnitude lower than those for $\Delta n > 0$ transitions, Boltzmann populations with respect to the ground state are already achieved for rather low electron densities. For example, for Be, at densities of about 10^{15} cm^{-3}, the population of the excited state $1s^2 2p$ is more important than that of the ground state $1s^2 2s$.[46] Therefore, all excited states of beryllium (e.g., for tokamaks at typical divertor densities) make larger contributions than the ground state.

The excited-state contribution could even be important at very low densities if the excited states are metastable states. Therefore, for heavy ions, where we encounter excited states that are close to ground states, related either by a dipole-allowed radiative transition or by multipole transitions, DR is extremely complex even at rather low densities. This is the main reason why, to date, ionic balance calculations of heavy elements differ strongly from one method to another and why DR remains an active field of research and of considerable interest for a number of applications (nuclear fusion, astrophysics, radiation sources, spectroscopic diagnostics, etc.).

In conclusion, the excited-state contribution is driven by atomic kinetics that can have a much greater impact than any other complicated effects related to ground-state contributions. This points again to the great practical importance of approximate methods, including the quasiclassical approach, that provide the possibility of obtaining numerical data even for large quantum numbers (which can be quite important for DR).

We underline that the excited-state contributions to DR up to high quantum numbers for the corresponding core transitions may exceed the ground-state contribution by many orders of magnitude. It is for this reason that it is essential to include excited-state contributions as much as possible, even if these are based on atomic structure calculations of limited precision, rather than attempting to improve via sophisticated atomic structure calculations the simplest core-transition-related DR rates while ignoring higher-order and excited-state contributions.

V. ANGULAR-MOMENTUM-CHANGING COLLISIONS

A strict consideration of angular-momentum-changing collisions requires a very extended atomic-level system that includes all details of the autoionizing states in order to treat properly the collisional redistribution of populations. We restrict ourselves here to a discussion of principles with the help of the most frequently employed formula for DR and proceed from dielectronic capture from channel k and with radiative transition $j \rightarrow i$ [see also Eqs. (3.3)–(3.5)]:

$$\langle DR\rangle_{k,ji}^{Z+1,Z} \approx \frac{1}{2g_k^{Z+1}}\left(\frac{2\pi\hbar^2}{m_e}\right)^{3/2} \frac{g_j^Z \Gamma_{jk}^{Z,Z+1} A_{ji}^Z}{\sum_l A_{jl}^Z + \sum_k \Gamma_{jk}^{Z,Z+1}} \frac{\exp\left(-E_{kj}^{DC}/kT_e\right)}{(kT_e)^{3/2}}. \tag{5.1}$$

Let us now consider a simple illustrative example, namely the Ly$_\alpha$ dielectronic $2l2l'$ satellites of He-like ions and depict two levels, one that has very large autoionization rate and one that has a negligible one. For the first case, we consider the level $j' = 2p^2\,{}^1D_2$, $k = 1s\,{}^2S_{1/2}$ and the radiative transition $j' = 2p^2\,{}^1D_2 \rightarrow i' = 1s2p\,{}^1P_1$. Atomic structure calculations for carbon ($Z_n = 6$) deliver[37]

$$\Gamma^{Z,Z+1}_{j'k} = 2.5\times10^{14}\ \mathrm{s}^{-1}, A^{Z}_{j'i'} = 1.4\times10^{12}\ \mathrm{s}^{-1},$$

$$\sum_l A^{Z}_{j'l} = 1.4\times10^{13}\ \mathrm{s}^{-1}, \sum_k \Gamma^{Z,Z+1}_{j'k} = 2.5\times10^{14}\ \mathrm{s}^{-1}.$$

For the second case, we consider the autoionizing configuration $j = 2p^2\,{}^3P_1$, $k = 1s\,{}^2S_{1/2}$ and the radiative transition $j = 2p^2\,{}^3P_1 \rightarrow i = 1s2p\,{}^3P_2$. Atomic structure calculations (again for $Z_n = 6$) deliver

$$\Gamma^{Z,Z+1}_{jk} = 0, A^{Z}_{ji} = 6.0\times10^{11}\ \mathrm{s}^{-1},$$

$$\sum_l A^{Z}_{jl} = 1.4\times10^{12}\ \mathrm{s}^{-1}, \sum_k \Gamma^{Z,Z+1}_{jk} = 0,$$

from which it follows that $Q^{Z+1,Z}_{k,ji} = 0$.

Assuming a two-level system where only dielectronic capture and angular momentum changing collisions (characterized by the rate coefficient $C_{j'j}$) contribute, the atomic populations n^Z_j and $n^Z_{j'}$ are given by

$$n^Z_{j'}\left(\sum_l A^Z_{j'l} + \sum_k \Gamma^{Z,Z+1}_{j'k} + n_e C_{j'j}\right) = n^{Z+1}_k n_e \langle DC\rangle^{Z+1,Z}_{k,j'} + n_e n^Z_j C_{jj'}, \tag{5.2}$$

$$n^Z_{j}\left(\sum_l A^Z_{jl} + \sum_k \Gamma^{Z,Z+1}_{jk} + n_e C_{jj'}\right) = n^{Z+1}_k n_e \langle DC\rangle^{Z+1,Z}_{k,j} + n_e n^Z_{j'} C_{j'j}, \tag{5.3}$$

where

$$\langle DC\rangle^{Z+1,Z}_{k,q} = \frac{1}{2g^{Z+1}_k}\left(\frac{2\pi\hbar^2}{m_e}\right)^{3/2} g^Z_q \Gamma^{Z,Z+1}_{qk} \frac{\exp\left(-E^{DC}_{kq}\big/kT_e\right)}{(kT_e)^{3/2}}, \tag{5.4}$$

with $q = j, j'$. In the absence of collisions, Eqs. (5.1)–(5.4) become

$$n^{(0),Z}_q = n^{Z+1}_k n_e \frac{1}{2g^{Z+1}_k}\left(\frac{2\pi\hbar^2}{m_e}\right)^{3/2} \frac{g^Z_q \Gamma^{Z,Z+1}_{qk}}{\sum_l A^Z_{ql} + \sum_k \Gamma^{Z,Z+1}_{qk}} \frac{\exp\left(-E^{DC}_{kq}\big/kT_e\right)}{(kT_e)^{3/2}}, \tag{5.5}$$

where the superscript "(0)" indicates the low-density case. As can be seen from Eq. (5.5), the low-density dielectronic intensity satellite factor [Eq. (3.5)] is reproduced from Eq. (5.2) if the angular-momentum-changing collisions are negligible, i.e., if

$$\sum_l A^Z_{j'l} + \sum_k \Gamma^{Z,Z+1}_{j'k} \gg n_e C_{j'j}.$$

Note that for very closely spaced levels, ion–ion collisions might also be of importance.

To understand the effect of angular-momentum-changing collisions on the total DR rate, we need to consider the sum for the two levels, i.e.,

$$\langle DR_{\mathrm{coll}}\rangle^{Z+1,Z}_{\mathrm{tot}} = \langle DR_{\mathrm{coll}}\rangle^{Z+1,Z}_{k,ji} + \langle DR_{\mathrm{coll}}\rangle^{Z+1,Z}_{k,j'i'}, \tag{5.6}$$

where the subscript "coll" for the single DR rates $\langle DR_{\mathrm{coll}}\rangle^{Z+1,Z}_{k,ji}$ and $\langle DR_{\mathrm{coll}}\rangle^{Z+1,Z}_{k,j'i'}$ indicates that these rates include collisional processes. This has to be distinguished from Eq. (5.1), which is a low-density approximation. It is of principal interest to understand the change in DR due to collisions with reference to the low-density case, i.e., we consider the ratio

$$\frac{\langle DR_{\mathrm{coll}}\rangle^{Z+1,Z}_{\mathrm{tot}}}{\langle DR\rangle^{Z+1,Z}_{\mathrm{tot}}} = \frac{\langle DR_{\mathrm{coll}}\rangle^{Z+1,Z}_{k,ji} + \langle DR_{\mathrm{coll}}\rangle^{Z+1,Z}_{k,j'i'}}{\langle DR\rangle^{Z+1,Z}_{k,ji} + \langle DR\rangle^{Z+1,Z}_{k,j'i'}}. \tag{5.7}$$

The collisional DR rates cannot be determined from relations like Eq. (5.5) but need to be determined directly from the populations, i.e.,

$$\langle DR_{\mathrm{coll}}\rangle^{Z+1,Z}_{k,ji} \propto n^Z_j A^Z_{ji}, \tag{5.8}$$

because the product of the level population with the radiative decay is the rate at which the excited state decays to the ground state, which is equivalent to DR [note that the usual branching ratios that appear in formulas like Eq. (5.1) are already included via the equilibrium population] if the right-hand sides of Eqs. (5.2) and (5.3) are driven by dielectronic capture and angular-momentum-changing collisions between the autoionizing levels under consideration. Combining Eqs. (5.7) and (5.8), we obtain

$$\frac{\langle DR_{\mathrm{coll}}\rangle^{Z+1,Z}_{\mathrm{tot}}}{\langle DR\rangle^{Z+1,Z}_{\mathrm{tot}}} = \frac{n^Z_j A^Z_{ji} + n^Z_{j'} A^Z_{j'i'}}{n^{(0),Z}_j A^Z_{ji} + n^{(0),Z}_{j'} A^Z_{j'i'}}, \tag{5.9}$$

i.e.,

$$\frac{\langle DR_{\mathrm{coll}}\rangle^{Z+1,Z}_{\mathrm{tot}}}{\langle DR\rangle^{Z+1,Z}_{\mathrm{tot}}} = \frac{\dfrac{n^Z_{j'}}{n^{(0),Z}_{j'}} + \dfrac{n^Z_j A^Z_{ji}}{n^{(0),Z}_{j'} A^Z_{j'i'}}}{\dfrac{n^{(0),Z}_j A^Z_{ji}}{n^{(0),Z}_{j'} A^Z_{j'i'}} + 1}. \tag{5.10}$$

Because $E^{DC}_{kj} \approx E^{DC}_{kj'}$, we have for the population ratio in the low-density case (for the example given above)

$$\frac{n^{(0),Z}_j}{n^{(0),Z}_{j'}} \approx \frac{g^Z_j \Gamma^{Z,Z+1}_{jk}}{g^Z_{j'} \Gamma^{Z,Z+1}_{j'k}} \frac{\sum_l A^Z_{j'l} + \sum_k \Gamma^{Z,Z+1}_{j'k}}{\sum_l A^Z_{jl} + \sum_k \Gamma^{Z,Z+1}_{jk}} \approx 0, \tag{5.11}$$

since $\Gamma^{Z,Z+1}_{jk} \ll \Gamma^{Z,Z+1}_{j'k}$ and $\Gamma^{Z,Z+1}_{jk} \ll \sum_l A^Z_{jl}$ (see the above example). Therefore, population is essentially transferred by angular-momentum-changing collisions from level j' to level j, but not vice versa. Let us now consider the above example with the populations given by Eqs. (5.2) and (5.3):

$$n^Z_j\left(\sum_l A^Z_{jl} + n_e C_{jj'}\right) \approx n_e n^Z_{j'} C_{j'j} \tag{5.12}$$

and

$$n^Z_{j'}\left(\sum_l A^Z_{j'l} + \sum_k \Gamma^{Z,Z+1}_{j'k}\right) \approx n^{Z+1}_k n_e \langle DC\rangle^{Z+1,Z}_{k,j'}. \tag{5.13}$$

Equations (5.2), (5.3), and (5.8) indicate that for autoionizing levels with very large autoionization rates, the populations are close to the

low-density case. Equation (5.4) therefore corresponds to the low-density case [Eq. (5.5)], i.e.,

$$n_{j'}^{Z} \approx n_{j'}^{(0),Z}. \tag{5.14}$$

Substituting Eqs. (5.11), (5.12), and .(5.14) into Eq. (5.9), we obtain

$$\frac{\langle DR_{\rm coll}\rangle_{\rm tot}^{Z+1,Z}}{\langle DR\rangle_{\rm tot}^{Z+1,Z}} \approx 1 + \frac{n_e C_{j'j}}{\sum_l A_{jl}^{Z} + n_e C_{jj'}} \frac{A_{ji}^{Z}}{A_{j'i'}^{Z}}. \tag{5.15}$$

Because $g_{j'}C_{j'j} \approx g_j C_{jj'}$ for closely spaced levels, Eq. (5.15) takes the form

$$\frac{\langle DR_{\rm coll}\rangle_{\rm tot}^{Z+1,Z}}{\langle DR\rangle_{\rm tot}^{Z+1,Z}} \approx 1 + \frac{g_j^{Z}}{g_{j'}^{Z}} \frac{A_{ji}^{Z}}{A_{j'i'}^{Z}} \left(\frac{1}{1 + \sum_l A_{jl}^{Z} \Big/ n_e C_{jj'}} \right). \tag{5.16}$$

If $\sum_l A_{jl}^{Z} \approx n_e C_{jj'}$, then the term in parentheses in Eq. (5.16) is about one-half, and the relation indicates that the total DR rate is enhanced (i.e., $\langle DR_{\rm coll}\rangle_{\rm tot}^{Z+1,Z}/\langle DR\rangle_{\rm tot}^{Z+1,Z} > 1$) owing to angular-momentum-changing collisions. This can be understood in a transparent qualitative picture: for the level j' with high autoionization rate, the dielectronic capture is high and, owing to the large autoionization rate, the branching factor for radiative deexcitation is small. If, however, a certain fraction of population is collisionally transferred to another level before autoionization and radiative decay disintegrate the upper level j', then level j is effectively populated by collisions from $j' \rightarrow j$ (because the population of level j is small since dielectronic capture is insignificant owing to a small autoionization rate). The transferred population, however, has a very favorable branching factor for level j compared with level j'. In the above example,

$$A_{ji}^{Z} \Big/ \left(\sum_l A_{jl}^{Z} + \sum_k \Gamma_{jk}^{Z,Z+1} \right) = 6.0\times10^{11} \Big/ 1.4\times10^{12} = 0.43$$

for level j, whereas

$$A_{j'i'}^{Z} \Big/ \left(\sum_l A_{j'l}^{Z} + \sum_k \Gamma_{j'k}^{Z,Z+1} \right) = 1.4\times10^{12} \Big/ 2.6\times10^{14} = 0.0088$$

for level j'. Therefore, the transferred population is more effectively transferred to the ground state to finally contribute to DR.

The impact of angular-momentum-changing collisions on the total DR rate is difficult to observe in dense plasmas, because the impact of such collisions is only indirect, namely, via the change in ionization balance, where other recombination processes (e.g., three-body recombination and radiative recombination) also come into play. However, angular-momentum-changing collisions can be directly observed via the collisional induced change in the spectral distribution of the corresponding dielectronic satellite transitions.

Figure 2 demonstrates this effect via He-like Ly_α transitions and their associated satellite transitions $2lnl' \rightarrow 1s2l + h\nu$. Numerical calculations of the spectral distribution have been carried out using the MARIA suite of codes,[10,47–49] taking into account an extended level structure, with *LSJ*-split levels of different ionization stages for ground, single, and multiple excited states being simultaneously included. Strong density effects are indicated by red arrows in Fig. 2.

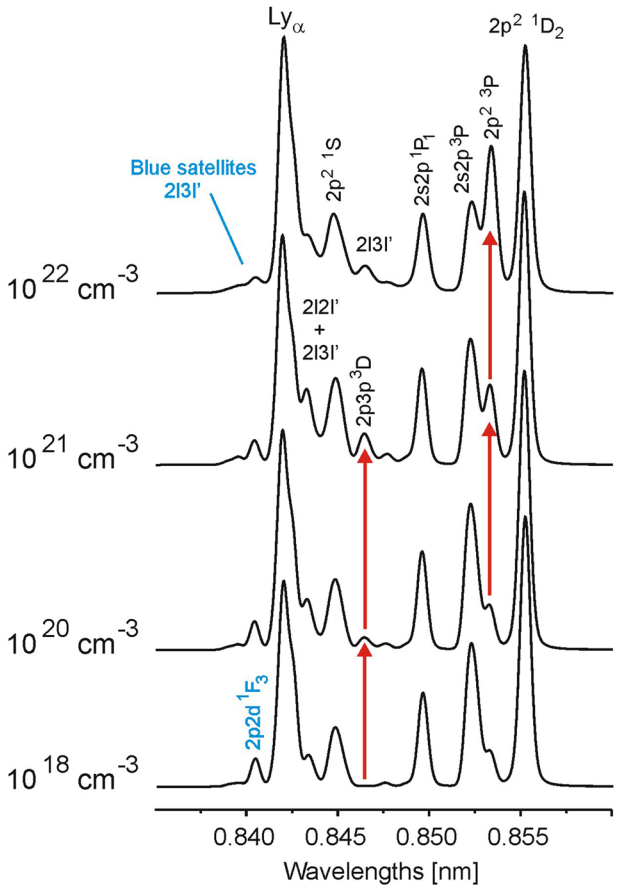

FIG. 2. MARIA simulations of dielectronic satellite emission near Ly_α of H-like Mg ions for different values of the electron density at kT_e = 100 eV. The red arrows indicate the rises in intensity of particular satellite transitions with increasing density. Satellites indicated in blue have effective negative screening due to strong angular-momentum coupling effects.

Not only do the $2l2l'$ satellites show strong density effects near $\lambda \approx 0.853$ nm, but so do the $2l3l'$ satellites near $\lambda \approx 0.847$ nm. The density sensitivity of the $2l3l'$ satellites starts at lower densities, because the collisional rates between the $2l3l'$ configurations are in general larger than those for the $2l2l'$ configurations [the collisional rates $C(2lnl'–2lnl'')$ increase with principal quantum number n, the corresponding radiative rates $A(2lnl''–1snl'')$ are almost independent of n, and the autoionization rates $\Gamma(2lnl''–1s)$ decrease with n]. Also indicated in Fig. 2 is the so-called "blue satellite" emission located on the blue wing of the Ly_α resonance line. These satellite transitions exhibit negative screening[7] that is due to the strong effect of angular-momentum coupling (F states). [Note that the term "negative screening" arises from use of the Bohr formula

$$E = \frac{Z_{\rm eff}^2 Ry}{n^2} = \frac{(Z_n - \sigma)^2 Ry}{n^2}$$

to match the actual energy E via a screening constant σ: in cases where the match can only be obtained for effective charges $Z_{\rm eff} = Z_n - \sigma$, the

screening constant is negative; see also Ref. 12.] As can be seen from Fig. 2, angular-momentum-changing collisions have little effect on blue satellites (because their autoionization rates are quite large).

In dense-plasma spectroscopy, the perturbation of the spectral dielectronic satellite distribution due to angular-momentum-changing collisions is employed for density diagnostics.[5–7] Note that although the satellite intensity shows variations with temperature too, density determination via dielectronic satellite transitions is essentially *not* a two-parameter problem: the temperature determination relies on the intensities of satellite transitions (with high autoionization rates) relative to the resonance line, while the density determination is based on the relative intensities of dielectronic satellites among the transitions themselves (with low and high autoionization rates). The density diagnostic is usually rather independent of the electron temperature, because all cross sections of angular-momentum-changing collisions are typically in the Born limit (the energy differences are typically much smaller than the electron temperature).

VI. ELECTRIC FIELD EFFECTS

A. Ionization potential depression of spectator electron orbitals

Atomic population kinetics of gases and plasmas has been applied very successfully to the study of low-density environments, where atoms and ions are essentially field-free. As the density increases, however, the free-atom model breaks down, resulting in a perturbation of the atomic energy levels. This perturbation manifests itself essentially in a broadening and a shift. Such perturbations can be observed in high-resolution spectroscopic experiments via analysis of the line broadening, the line shift, and the disappearance of the line emission corresponding to the ionization potential depression (IPD) of the upper level. The IPD is of great interest for applications in thermodynamics and also for the understanding of various radiative properties, such as emission, absorption, and scattering (for further reading on current developments in IPD research with spectroscopic precision, the interested reader is referred to Refs. 50 and 51 and references therein).

The fundamental origin of the perturbation of energy levels is the plasma electric microfield, which in turn also limits the number of bound states. Electric field ionization starts at a critical field strength $F_{\rm crit}$ given by[39,52]

$$F_{\rm crit} \approx 6.8\times 10^8 \frac{Z_{\rm eff}^3}{n_F^4}\ [\rm V/cm], \tag{6.1}$$

where $Z_{\rm eff}$ is the effective ion charge and n_F is the principal quantum number at which field ionization starts. To estimate the limited number of quantum states that effectively take part in the recombination process, we identify the critical field strength $F_{\rm crit}$ with the mean field strength, which can be expressed in terms of the Holtsmark normal mean field strength F_0 (Z_P is the perturber charge and N_P is the perturber density),[52a]

$$\begin{aligned} F_{\rm mean} &\approx 3.41F_0 = 3.4\times 4\pi\left(\frac{4}{15}\right)^{2/3}\left(\frac{Ry}{e}\right)a_0 Z_P N_P^{2/3} \\ &\approx 1.3\times 10^{-6} Z_P N_P^{2/3}\ [\rm cm^{-3}]\,[V/cm], \end{aligned} \tag{6.2}$$

and we identify the principal quantum number n_F with the maximum principal quantum number of the spectator electron nl of the autoionizing configuration, i.e.,

$$n_F \approx n_{\rm max}^{\rm spectator} \approx 4.8\times 10^3 \frac{Z_{\rm eff}^{3/4}}{Z_P^{1/4} N_P^{1/6}\ (\rm cm^{-3})}. \tag{6.3}$$

$n_{\rm max}^{\rm spectator}$ limits the contribution of high-n spectator electrons according to Eq. (3.17) [and therefore effectively limits the B_d values in Eqs. (3.14), (3.15), and .(3.20)]. Equation (6.3) is useful to understand the various effects that limit DR (apart from the electric field effect, kinetic effects, for example, may likewise limit the effective rate coefficient; see below). Note, however, that Eq. (6.3) itself provides only a rough estimate of the principal quantum number of the spectator electrons due to the electric field effect, since (a) it neglects the fact that usually up to five perturber charge states are present in a dense plasma, (b) the field strength distribution is only taken into account via the mean field value, and (c) charged-particle correlations that influence the field strength distribution itself are ignored.

Effective DR is not only limited by the maximum principal quantum number $n_{\rm max}^{\rm spectator}$ from Eq. (6.3), but also by collisional disintegration of the autoionizing level: in fact, in a dense plasma, not only does the high density of charged particles result in a high microfield, but the high density also implies a significant rate of collisional processes. For autoionizing states, we need to consider two stages: a first stage involving collisional processes associated with core relaxation and a second stage following core relaxation. Concerning the first stage, we need to compare the radiative stabilization rate of the autoionizing configuration (which is the origin of effective recombination) with the collisional ionization rate of the spectator electron (which is the origin of collisional disintegration of the autoionizing level). Therefore, effective DR requires

$$A_{\rm rad}(\alpha\to\alpha_0) \gg n_e I_n, \tag{6.4}$$

where $A_{\rm rad}(\alpha\to\alpha_0)$ is the radiative stabilization rate from Eqs. (3.10) and (3.20) (note that this rate is distinctly different from the radiative transition rate of the spectator electron itself), n_e is the electron density, and I_n is the electron collisional ionization rate coefficient of the spectator electron with principal quantum number n. Note that for autoionizing states, the stabilization rate is almost independent of the high-n spectator electron, which is distinctly different from the scaling law for singly excited states (approximately $A\propto 1/n^3$). If the radiative stabilization is associated with a change in principal quantum number, then the H-like approximation can be used to estimate $A_{\rm rad}(\alpha\to\alpha_0)$:

$$A_{\rm rad}(\alpha\to\alpha_0, \Delta n>0) \approx \frac{1.57\times 10^{10} Z_{\rm eff}^4}{n_{\alpha 0} n_\alpha^3 (n_\alpha^2 - n_{\alpha 0}^2)}\ [\rm s^{-1}], \tag{6.5}$$

where $Z_{\rm eff}$ is the effective ion charge. If $A_{\rm rad}(\alpha\to\alpha_0)$ is associated with a transition without change in principal quantum number, i.e., $\Delta n=0$, then numerical Hartree–Fock calculations including angular-momentum coupling are required to obtain reasonable estimates of the transition probability. Numerical calculations indicate that for Li-like and Be-like ions, transition probabilities and oscillator strengths can be roughly estimated from the expressions

$$A_{\rm rad}(1s^2 2p\ ^2P \to 1s^2 2s\ ^2S) \approx 1.2\times 10^8 (Z_n - 3)\ (\rm s^{-1}),$$

$$f\,(1s^2 2s\,{}^2S \rightarrow 1s^2 2p\,{}^2P) \approx 1.2/\,(Z_n - 2),$$

$$A_{\rm rad}\,(1s^2 2s2p\,{}^1P \rightarrow 1s^2 2s^2\,{}^1S) \approx 8\times 10^8\,(Z_n - 3)\ [{\rm s}^{-1}],$$

$$f\,(1s^2 2s^2\,{}^1S \rightarrow 1s^2 2s2p\,{}^1P) \approx 4.5/\,(Z_n - 2).$$

The ionization rate of the spectator electron can be estimated from the following expression (note that there are many competing formulas available in the literature,[26] but for the present estimates, the simple Lotz-like formula appears to provide a good balance between complexity and precision):

$$I_n \approx 6\times 10^{-8}\left(\frac{Ry}{E_n}\right)^{3/2}\sqrt{\beta_n}\,e^{-\beta_n}\ln\left[1+\frac{0.562+1.4\beta_n}{\beta_n(1+1.4\beta_n)}\right]\ [{\rm cm}^3/{\rm s}], \tag{6.6}$$

where $Ry = 13.6056$ eV and

$$\beta_n = \frac{E_n}{kT_e}. \tag{6.7}$$

E_n is the ionization potential of the spectator electron, which can be approximated by

$$E_n \approx \frac{(Z_{\rm eff}-1)^2 Ry}{n^2}. \tag{6.8}$$

It is important to point out that the condition (6.4) is necessary for DR to be effective, but it is *not* sufficient. After radiative stabilization $\alpha \rightarrow \alpha_0$ of the core, we need to radiatively stabilize the spectator electron nl to the ground state "gr" (if it disappears in the continuum, no recombination is encountered), i.e., we must have

$$A_{\rm rad}\,(nl \rightarrow {\rm gr}) \gg n_e I_n. \tag{6.9}$$

For spectator electrons, $\Delta n = 0$ transitions are not relevant and an expression similar to Eq. (6.5) describes all cases of practical interest:

$$A_{\rm rad}\,(nl \rightarrow {\rm gr}, \Delta n > 0) \approx \frac{1.57\times 10^{10}\,(Z_{\rm eff}-1)^4}{n_{\rm gr} n^3\,(n^2 - n_{\rm gr}^2)}\ [{\rm s}^{-1}]. \tag{6.10}$$

Whether condition (6.4) or (6.9) is more stringent depends on the type of core transition. Let us consider as an example a magnetically confined deuterium fusion plasma containing Li-like iron impurities. Assuming $Z_P = 2$, $N_P = 10^{13}$ cm^{-3}, $n_e = 10^{14}$ cm^{-3}, and $kT_e = 10$ keV, we obtain from Eq. (6.3) with $Z_{\rm eff} = 24$ a maximum principal quantum number of spectator electrons of about $n_{\rm max}^{\rm spectator} \approx 300$. For Li-like iron, DR is associated with the core transition $\alpha_0 \rightarrow \alpha = 1s^2 2s\,{}^2S \rightarrow 1s^2 2p\,{}^2P$ with $A_{\rm rad}(1s^2 2p\,{}^2P \rightarrow 1s^2 2s\,{}^2S) \approx 3.5\times 10^9$ s^{-1} and $f(1s^2 2s\,{}^2S \rightarrow 1s^2 2p\,{}^2P) \approx 0.066$. As the relevant principal quantum numbers are of the order of 100, we have

$$\beta_n = \frac{E_n}{kT_e} = \frac{(24-1)^2\times 13.6}{10^4 n^2} \approx 10^{-4},$$

and we can approximate the β_n-dependent terms in Eq. (6.6) roughly by 0.1 and solve Eq. (6.4) for the critical principal quantum number of the spectator electron $n_{\rm crit}^{\rm spectator}$ [note that the critical principal quantum number is obtained from Eq. (6.4) with equality sign]: $n_{\rm crit}^{\rm spectator} \approx (7\times 10^{21}/n_e)^{1/3} \approx 400$.

Let us now investigate the condition (6.9). For Li-like iron, $n_{\rm gr} = 2$ and Eq. (6.10) provides roughly $A_{\rm rad}(nl \rightarrow {\rm gr}, \Delta n > 0) \approx 2\times 10^{15}/n^5$ [s^{-1}]. Taking into account the n dependence of $A_{\rm rad}(nl \rightarrow {\rm gr}, \Delta n > 0)$, we can solve Eq. (6.9) for the critical principal quantum number $n_{\rm crit}^{\rm spectator}$ [note that the critical principal quantum number is obtained from Eq. (6.10) with equality sign] of the spectator electron: $n_{\rm crit}^{\rm spectator} \approx (4\times 10^{23}/n_e)^{1/8} \approx 16$. Therefore, in the above example, the condition (6.10) is much more stringent than conditions (6.3) and (6.4).

Let us now consider the above example for parameters typical of inertial fusion plasmas. We assume that iron is employed as a -diagnostic tracer element in a compressed dense plasma. Assuming $Z_P = 2$, $N_P = 10^{23}$ cm^{-3}, $n_e = 10^{25}$ cm^{-3}, and $kT_e = 10$ keV, we obtain from Eq. (6.3) with $Z_{\rm eff} = 24$ a maximum principal quantum number of the spectator electron of about $n_{\rm max}^{\rm spectator} \approx 6$. As before, $\alpha_0 \rightarrow \alpha = 1s^2 2s\,{}^2S \rightarrow 1s^2 2p\,{}^2P$ with $A_{\rm rad}(1s^2 2p\,{}^2P \rightarrow 1s^2 2s\,{}^2S) \approx 3.5\times 10^9$ s^{-1} and $f(1s^2 2s\,{}^2S \rightarrow 1s^2 2p\,{}^2P) \approx 0.066$. As the relevant principal quantum numbers are of the order of 10, we have

$$\beta_n = \frac{E_n}{kT_e} = \frac{(24-1)^2\times 13.6}{10^4 n^2} \approx 10^{-2},$$

and we can approximate the β_n-dependent terms in Eq. (6.6) roughly by 0.4 and solve Eq. (6.4) for the critical principal quantum number of the spectator electron $n_{\rm crit}^{\rm spectator}$ [note that the critical principal quantum number is obtained from Eq. (6.4) with equality sign]: $n_{\rm crit}^{\rm spectator} \approx (2\times 10^{21}/n_e)^{1/3} < 1$. Therefore, DR associated with the Li-like core transition $\alpha_0 \rightarrow \alpha = 1s^2 2s\,{}^2S \rightarrow 1s^2 2p\,{}^2P$ is ineffective. The essential physical reason is related to the low transition probability for the $\Delta n = 0$ core transition. Therefore, total recombination rates are effectively related to core transitions involving the K shell because, in this case, the radiative decay rates are very large owing to the strong Z scaling [see Eq. (6.5)]: assuming $Z_{\rm eff} = 24$ as before, but taking $n_{\alpha 0} = 1$ and $n_\alpha = 2$ in Eq. (6.5), we have $A_{\rm rad}(\alpha \rightarrow \alpha_0, \Delta n > 0) \approx 1.1\times 10^{14}$ s^{-1}, i.e., a value five orders of magnitude higher compared with the $\Delta n = 0$ core transition discussed above. In this case, K-electron involvement in a core transition allows a few principal quantum numbers of the order of 1 to survive and to contribute effectively to DR.

What is the conclusion from the above estimates? They indicate that it might not be appropriate to adopt a purely atomic structure point of view to obtain convergence of the sum of DR rates over a large range of principal quantum numbers of the spectator electron nl in Eq. (3.17): owing to microfields and collisional–radiative competition, large principal quantum numbers might not effectively contribute to the total DR rate. Therefore, total DR rates calculated with rather approximate methods (quasiclassical methods or Vainshtein's simplified QMMC method) but taking into account the plasma microfield and collisional processes might be more accurate than purely adopting sophisticated atomic structure calculations.

In view of these results, we now address the influence of the plasma microfield itself on the autoionization rates.

B. Perturbed autoionization rates

The influence of the electric field on the autoionization and corresponding DR rates was first studied in Refs. 53–55 in the context of the simplest atomic system of He-like autoionizing states $2l2l'$. It

was realized that forbidden autoionizing processes (i.e., forbidden in the *LS*-coupling scheme) become allowed by electric field mixing of autoionizing bound-state wavefunctions. The allowed autoionization width is given by the first-order transition rate

$$\Gamma(d \to c) = \frac{2\pi}{\hbar} |\langle d|V|c\rangle|^2 \delta(E_d - E_c), \tag{6.11}$$

where V is the electrostatic interaction. Because V is a scalar operator, the autoionization vanishes unless there are available adjacent continuum states c with the same angular momentum and parity as those of the discrete levels d.[32] Because of the absence of even-parity P states below the second ionization threshold, the $2p^2\ ^3P$-state of He-like ions is metastable against autoionization decay. In the presence of perturbing electric fields, however, autoionization of the state $a = 2p^2\ ^3P$ may occur by a second-order process involving a field-induced transition to the nearby autoionizing state $d = 2s2p\ ^3P$. In a quasistatic ion field, the field-induced autoionization rate is given by

$$\Gamma(a \to c) = \frac{2\pi}{\hbar} \left| \sum_d \frac{\langle a \mid \vec{Q} \cdot \vec{E} \mid d\rangle \langle d \mid V \mid c\rangle}{(E_a - E_d) + i\hbar(\Gamma_d + A_d)/2} \right|^2 \delta(E_a - E_c), \tag{6.12}$$

where $\vec{Q}$ is the electric dipole moment operator, and Γ_d and A_d are respectively the autoionization and radiative widths of the state d. Therefore, the first-order contribution from the field-induced transition decays directly into the nonresonant continuum $c = 1s\varepsilon p\ ^3P$.

It should be noted that for practical applications, not only field-induced transitions have to be considered, but intermediate coupling, configuration, and magnetic interactions too. In particular for highly charged ions, these "non-electric-field effects" may make a considerable contribution to the forbidden autoionization width, as is demonstrated by the results in Table VI, which have been calculated using the FAC code.[56] In addition, the Breit interaction[56a] induces an autoionization rate for the $2p^2\ ^3P_1$ state.

Table VI also illustrates the general effect that if the nuclear charge increases, then the autoionization widths are more evenly distributed over the levels. Therefore, electric field effects are best studied for low-Z elements. The table also demonstrates that autoionization rates are strongly dependent on *LSJ* quantum numbers: therefore, simple summations over l quantum numbers might be a quite inappropriate way to simplify complex atomic structures in kinetics.[48]

From the relationship between the corresponding capture and autoionization rates, it follows that the electric field can induce DR through normally inaccessible high-angular-momentum states that have large statistical weights.[54,55] In fact, in a plasma, the angular momentum l is no longer a good quantum number, because the presence of an electric field destroys the spherical symmetry. However, the projection L_Z of L , which generates the magnetic quantum number m, defined with respect to the direction of the electric field, remains a good quantum number. For nonzero quantum numbers m, this results in a twofold degeneracy of the outer electrons in addition to the twofold degeneracy due to spin. The appropriate transformation of the field-free substates l has the form

$$|n\lambda m\rangle = \sum_{l=|m|}^{n-1} |nlm\rangle \langle nlm, |n\lambda m\rangle\rangle, \tag{6.13}$$

where the electric quantum number λ, which replaces l in the presence of the electric field, can take integer values in the range $\lambda = 0, \ldots, n - |m| - 1$. Calculations[54,55,57,58] demonstrate that the dependence of the autoionization rates on the quantum number λ is rather smooth, in contrast to the field-free case, where the autoionization rates decrease rapidly with quantum number l. For this reason, dielectronic capture increases in the presence of an electric field, because it is proportional to the autoionization rate and the statistical weight: $\langle DC\rangle_{k,j}^{Z+1,Z} \propto g_j^Z \Gamma_{jk}^{Z,Z+1}$. Because the DR rate is proportional to dielectronic capture rate [see Eq. (2.7)], this results in a considerable increase in the total DR rate. For example, for the autoionizing states $1s^2 2pnl$ in Be-like Fe^{22+}, an approximately threefold increase in the DR rate was found even for densities as low as 10^{14} cm^{-3}.[54] This dramatic increase at rather low densities is connected in particular with the fact that for the $1s^2 2pnl$ configuration, the resonance spontaneous transition probability $2s$–$2p$ is not very large and high-n states have autoionization rates larger than radiative decay rates for n quantum numbers up to about 100. Consequently, high-n states contribute considerably to the DR rate. As high-n states are likewise strongly affected by rather small electric fields, a considerable impact on the total recombination rate is encountered even for rather low plasma densities (being of importance for typical densities of the solar corona or magnetic fusion plasmas).

Interaction with an electric field makes atomic structure calculations extremely complex, and it is difficult to derive general conclusions. However, it has been demonstrated[57,58] that the quasiclassical approach combined with a transformation to parabolic quantum numbers [Eq. (6.13)] gives results that are in surprisingly good agreement with those of extremely complex numerical calculations.[59] Moreover, the quasiclassical approach combined with the transformation to parabolic quantum numbers[59a,59b] enables the derivation of a closed-form expression for the autoionization rate in an electric field:

TABLE VI. Field-free autoionization decay rates (s^{-1}) including intermediate coupling, configuration, and magnetic interaction.

State	$Z_n = 3$	$Z_n = 6$	$Z_n = 13$	$Z_n = 18$	$Z_n = 26$	$Z_n = 42$
$2p^2\ ^1S_0$	8.4×10^{10}	5.1×10^{12}	1.3×10^{13}	1.9×10^{13}	3.4×10^{13}	7.0×10^{13}
$2p^2\ ^1D_2$	1.5×10^{14}	2.5×10^{14}	3.1×10^{14}	3.1×10^{14}	2.3×10^{14}	2.1×10^{14}
$2p^2\ ^3P_0$	2.9×10^{7}	2.3×10^{9}	2.3×10^{11}	1.2×10^{12}	3.7×10^{12}	2.8×10^{12}
$2p^2\ ^3P_1$	0	0	0	0	0	0
$2p^2\ ^3P_1$ with Breit interaction	2.6×10^{7}	6.8×10^{8}	1.9×10^{10}	7.2×10^{10}	3.2×10^{11}	2.2×10^{12}
$2p^2\ ^3P_2$	1.1×10^{9}	3.1×10^{10}	3.0×10^{12}	2.1×10^{13}	1.1×10^{14}	1.5×10^{14}

$$\Gamma(n,\lambda,m) = \int_{l_{\min}}^{l_{\max}} P(nl;\lambda m)\Gamma(nl)\,dl, \tag{6.14}$$

with

$$l_{\min}^2 = \frac{1}{2}\left\{[(n-1)^2 + m^2 - \lambda^2] - \sqrt{[(n-1)^2 + m^2 - \lambda^2]^2 - 4(n-1)^2 m^2}\right\} \tag{6.15}$$

and

$$l_{\max}^2 = \frac{1}{2}\left\{[(n-1)^2 + m^2 - \lambda^2] + \sqrt{[(n-1)^2 + m^2 - \lambda^2]^2 - 4(n-1)^2 m^2}\right\}, \tag{6.16}$$

where $\Gamma(nl)$ is the standard autoionization rate in spherical polar coordinates (which is independent of m owing to spherical symmetry) and $P(nl;\lambda m)$ is a joint probability (with normalization equal to unity) for the appearance of spherical (nl) and parabolic $(n\lambda m)$ quantum numbers that can be expressed in terms of Clebsch–Gordan coefficients. For large quantum numbers and the condition $m < l \ll n$ (the quasiclassical limit of Clebsch–Gordan coefficients that is of practical interest), the joint probability can be approximated by[58]

$$P(nl;\lambda m) \approx \frac{1}{\pi}\frac{2l}{\sqrt{(l^2 - l_{\min}^2)(l_{\max}^2 - l^2)}}. \tag{6.17}$$

Substituting quasiclassical values for the autoionization rate[31,32,36,38,42] $\Gamma(nl)$ into Eq. (6.14) and using Eq. (6.13), we obtain an autoionization rate in parabolic quantum numbers expressed in terms of universal functions ($t = l/l_{\text{eff}}$, $l_{\text{eff}} = (3Z^2/\omega)^{1/3}$):

$$\Gamma(n,\lambda,m) = \frac{f_{ij}}{\pi n^3} I(t_{\min}, t_{\max}), \tag{6.18}$$

$$I(t_{\min}, t_{\max}) \approx \frac{2}{l_{\max}}\left(\frac{3Z^2}{\omega}\right)^{2/3} Y\left(l_{\min}(\omega/3Z^2)^{1/3}\right), \tag{6.19}$$

$$Y(x) \approx 0.284\exp(-2x^3), \tag{6.20}$$

where f_{ij} is the oscillator strength of the core transition with charge Z (e.g., the oscillator strength corresponding to the transition $1s$–$2p$ in H-like Al for the He-like $2\text{nl}'$ satellites, $Z = 13$). The expressions (6.14)–(6.20) demonstrate similarly a broad distribution over the electric quantum number λ that finally results in an increase of the DR rate.

VII. THE LOCAL PLASMA FREQUENCY APPROACH TO DIELECTRONIC RECOMBINATION

As discussed already, DR is the most effective recombination channel in electron–heavy-ion collisions. Owing to the complex electronic structure of multielectron ions, providing a proper account of all necessary channels is a very difficult task, in particular for open-shell configurations. In addition, in dense plasmas, dielectronic capture might effectively proceed from excited states (see also Sec. IV), thus considerably increasing the number of quantum channels for dielectronic capture. Moreover, in heavy ions, numerous metastable states may play the role of excited states even in rather low-density plasmas, thereby increasing the numerical complexity of fully quantum calculations considerably. At present, DR of heavy ions is still a matter of controversy and is one of the main sources of discrepancy between different methods of calculation for radiation loss and ionic charge state distributions. It is therefore of great interest to develop different methods for the calculation of the DR rate in heavy ions that permit more general studies, including analysis of scaling laws. Below, we develop a twofold statistical approach that is realized by a combination of the statistical theory of atoms[60–65] with the local plasma frequency approximation.[40,41,66]

Let us start from Eq. (3.4) and rewrite the formula for the total DR rate as

$$\langle DR(T_e)\rangle = \left(\frac{4\pi Ry}{kT_e}\right)^{3/2} \times a_0^3 \frac{g_f}{g_i} A \sum_{n,l}\left[\frac{\Gamma(n,l)}{A + \Gamma(n,l)}\exp\left(-\frac{\hbar\omega}{kT_e} + \frac{Z_i^2 Ry}{n^2 kT_e}\right)\right], \tag{7.1}$$

where kT_e is the electronic temperature in eV, g_i and g_f are the statistical weights of the initial and final states of the atomic core, A is the radiative transition probability inside the core, Γ is the autoionization decay rate of an excited atomic energy level, $\hbar\omega$ is the transition energy inside the core, Z_i is the ion charge, a_0 is the Bohr radius, and n and l are the principal and orbital quantum numbers, respectively, of the captured electron. The radiative decay rate is expressed simply in terms of the oscillator strength f_{ij} for the transition inside the core:

$$A = \frac{2\omega^2 f_{if}}{c^3}, \tag{7.2}$$

where c is the speed of light. To obtain an expression for the autoionization decay rate $\Gamma(n, l)$, we use a relationship between the decay rate $\Gamma(n, l)$ and the partial electron excitation cross section $\sigma_{\text{ex}}(n, l)$ in the semiclassical representation. The quantities $\Gamma(n, l)$ and $\sigma_{\text{ex}}(n, l)$ describe mutually inverse processes, so the relationship between them can be obtained from the detailed balance between ions X^{Z_i+1} and X^{Z_i}. Thus, we obtain

$$(2l+1)g_f\Gamma(n,l) = \frac{Z^2}{n^3}\omega g_i \frac{\sigma_{\text{ex}}(n,l)}{\pi^2 a_0^2}. \tag{7.3}$$

The electron excitation cross section in the semiclassical approximation takes the form

$$\sigma_{\text{ex}}(n,l) = \frac{8\pi}{3}\left(\frac{\hbar}{mV_e}\right)^2 \frac{g_f}{g_i} f_{if} Z_i^{-2}(l+\frac{1}{2})^2 G\left(\frac{\omega(l+\frac{1}{2})^3}{3Z_i^2}\right), \tag{7.4}$$

where the function $G(u)$ is given by

$$G(u) = u[K_{1/3}^2(u) + K_{2/3}^2(u)], \tag{7.5}$$

where $K_{1/2}$ and $K_{3/2}$ are the Macdonald functions (modified Bessel functions of the second kind). Taking into account that the essential values of the argument of the function $G(u)$ are never close to zero, it is possible to replace $G(u)$ by its asymptotic expansion:

$$G(u) \approx 3.4\exp(-2u). \tag{7.6}$$

With these approximations, the autoionization decay rate takes the form

$$\Gamma(n,l) \approx 0.72\frac{\omega\left(l+\frac{1}{2}\right)f_{ij}}{n^3}\exp\left[-\frac{2\omega(l+\frac{1}{2})^3}{3Z_i^2}\right]. \tag{7.7}$$

The sum of the absorption oscillator strengths satisfies the Thomas–Reiche–Kuhn sum rule, i.e.,

$$N_e = \sum_f f_{if} \tag{7.8}$$

(note that N_e is the number of electrons, while n_e is the electron density and n the principal quantum number). In the statistical model, the oscillator strengths are expressed in terms of the atomic electron density $n_e(r, q, Z_n)$, and the statistical sum rule is given by

$$N_e = \int n_e(r,q,Z_n)\,dV. \tag{7.9}$$

The application of the semiclassical statistical model to the general formula (7.1) for the total DR is achieved by using the relationships

$$\sum_f f_{if} \to \int_0^{r_0} dr\ 4\pi r^2 n_e(r,q,Z_n) \tag{7.10}$$

and

$$E_{if} \to \omega = \sqrt{4\pi n_e(r,q,Z_n)}. \tag{7.11}$$

After all the substitutions, we obtain for the DR rates

$$\langle DR[\mathrm{cm}^3/\mathrm{s}]\rangle = 0.61\times10^{-8}\langle DR(\mathrm{a.u.})\rangle, \tag{7.12}$$

$$\langle DR(\mathrm{a.u.})\rangle = \frac{54.5}{T_e^{3/2}}\left(\frac{Z_n}{Z_i}\right)^2\int_0^{x_0} dx\ x^2\left[\frac{\varphi(x,q)}{x}\right]^{9/4} \times\int_1^{\infty} dt\ \exp\left[-\frac{\omega(x)}{T_e}\left(1-\frac{1}{t^2}\right)\right] \times\int_0^{l_{\max}=tn_1-1} dl\ \frac{(l+\frac{1}{2})\exp[-2\omega(x)(l+\frac{1}{2})^3/3Z_i^2]}{t^3+A(x,l)}, \tag{7.13}$$

$$A(x,l) = 5.2\times10^6\left(l+\frac{1}{2}\right)\frac{\exp\left[-2\omega(x)(l+\frac{1}{2})^3/3Z_i^2\right]}{Z_i^3\sqrt{\omega(x)}}, \tag{7.14}$$

$$\omega(x) = 1.2Z_n\left[\frac{\varphi(x,q)}{x}\right]^{3/4}, \tag{7.15}$$

with T_e[a.u.] = T_e[eV]/27.21 and $t = n/n_1$, where n_1 is the minimum possible quantum number. n_1 is the lowest level at which electron capture is possible and corresponds to an energy of an incident electron E_i, given by

$$E_i = \omega - \frac{Z_i^2}{2n^2}, \tag{7.16}$$

that is equal to zero, i.e.,

$$0 = \omega - \frac{Z_i^2}{2n_1^2}, \tag{7.17}$$

from which it follows that

$$n_1 = \frac{Z_i}{\sqrt{2\omega}}. \tag{7.18}$$

In the framework of the Thomas–Fermi model,[60–65] the electron density distribution of a particular element and charge state is given by

$$n_e(x,q,Z_n) = \frac{32}{9\pi^3}Z_n^2\left[\frac{\varphi(x,q)}{x}\right]^{3/2}, \tag{7.19}$$

with

$$x = \frac{r}{r_{\mathrm{TF}}}, \tag{7.20}$$

$$r_{\mathrm{TF}} = \left(\frac{9\pi^3}{128}\right)^{1/3}\frac{1}{Z_n^{1/3}} = 0.8853Z_n^{-1/3}, \tag{7.21}$$

$$q = \frac{Z}{Z_n}, \tag{7.22}$$

where Z_n is the nuclear charge, Z is the ion charge, q characterizes the degree of ionization, and r_{TF} is the Thomas–Fermi radius. The Thomas–Fermi function $\varphi(x, q)$ can be approximated by the Sommerfeld method[61,62,67] as an exact particular solution of the Thomas–Fermi differential equation:

$$\varphi(x,q) = \varphi_0(x)\left\{1-\left[\frac{1+z(x)}{1+z_0(x)}\right]^{\lambda_1/\lambda_2}\right\}, \tag{7.23}$$

with

$$z(x) = \left(\frac{x}{144^{3/2}}\right)^{\lambda_2}, \tag{7.24}$$

$$z_0(x) = \left[\frac{x_0(q)}{144^{3/2}}\right]^{\lambda_2}, \tag{7.25}$$

$$\varphi_0(x) = \frac{1}{[1+z(x)]^{\lambda_1/2}}, \tag{7.26}$$

$$\lambda_1 = 0.5\left(7+\sqrt{73}\right) = 7.77200, \tag{7.27}$$

$$\lambda_2 = 0.5\left(-7+\sqrt{73}\right) = 0.77200. \tag{7.28}$$

The reduced radius $x_0(q)$ is determined from the boundary condition

$$x_0\frac{d\varphi(x_0)}{dx} = -q. \tag{7.29}$$

In a high-temperature plasma, i.e., when the degree of ionization $q = Z/Z_n$ is not too low, the reduced radius can be approximated by

$$x_0(q) = \begin{cases} 2.96\left(\dfrac{1-q}{q}\right)^{2/3} & \text{if} \quad 0.2 < q \le 1, \\ 6.84\dfrac{1}{q^3} & \text{if} \quad q < 0.05. \end{cases} \tag{7.30}$$

Note that the use of the Thomas–Fermi model described above, which ignores exchange corrections, is quite appropriate within the framework of the approximations of the statistical DR model itself (see also the further discussion below). The ionization energy of an atom or ion is then given by

$$I_Z = Z_n^2 Ry\left\{\left(\frac{128}{9\pi^2}\right)^{1/3}\frac{2Z}{Z_n^{5/3}x_0(q,Z_n)}\right\}. \tag{7.31}$$

As can be seen from Eq. (7.31), the hydrogenic approximation $Z_n^2 Ry$ of the ionization potential of an ion with charge Z_n is corrected via the Thomas–Fermi electron density distribution, which depends on the nuclear and ionic charges [the factor in braces $\{\cdots\}$ in Eq. (7.31)]. A comparison of the ionization energies obtained from Eq. (7.31) with the results of detailed Hartree–Fock calculations shows reasonable agreement for heavy elements over a wide range of degrees of ionization.[66] Note that more accurate descriptions of the ionization potentials can certainly be obtained from a direct fit to the vast number of ionization potentials that are known as functions of Z and Z_n:[68]

$$I_Z \approx 0.221\, Ry\,\frac{(1+Z)^{4/3}}{1-0.96\left(\dfrac{1+Z}{Z_n}\right)^{0.257}}. \tag{7.32}$$

Many modifications of the Thomas–Fermi model have been proposed with the aim of including shell structure, obtaining improved ionization energies, and, in particular, approaching the Hartree–Fock results for the electron density distribution. In further developments to improve the statistical approach, however, one must not lose sight of the requirement that the fundamental equations of the statistical model of atoms, including the various corrections terms, should not be too complicated, in particular no more complicated than the basic equations of the quantum mechanical many-body approximation (e.g., the multiconfiguration Hartree–Fock methods). One must always bear in mind that the statistical theory of atoms is only a rough approximation of the quantum atom and that its advantage is its extreme simplicity both in structure and application to determine the electron and potential distributions of atoms, to derive elementary processes in collisional–radiative regimes, to shed light on detailed atomic structure calculations (in particular for heavy atoms), and, in particular, to derive general scaling laws that could hardly be obtained otherwise. It is this practical philosophy that we adopt when we consider Eqs. (7.19)–(7.31) for the statistical framework of the atom/ion and its realization via the local plasma frequency.

In the simplest version of the statistical model, the atomic density, excitation energies, and oscillator strengths do not depend on the orbital momentum quantum number l. If we average the branching factor over orbital momentum l, i.e.,

$$\sum_{n,l}\frac{\Gamma(n,l)}{A+\Gamma(n,l)},$$

then we obtain for the total DR rate

$$\langle DR(\text{a.u.})\rangle = \frac{39.2}{T_e^{3/2}}\left(\frac{Z_n}{Z_i}\right)^2\frac{Z_n}{Z_i^2}\int_0^{x_0}dx\; x^2\left[\frac{\varphi(x)}{x}\right]^3 \times\int_1^\infty\frac{dt}{t^2}\exp\left[-\frac{\omega(x)}{T}\left(1-\frac{1}{t^2}\right)\right] \times\int_0^{tn_1}dl\;\frac{(l+\frac{1}{2})^2\exp\left[-2\omega(x)(l+\frac{1}{2})^3\Big/3Z_i^2\right]}{t^3+A(x,l)}, \tag{7.33}$$

where the function $A(x,l)$ is given by Eqs. (7.14) and (7.15). Instead of averaging over the branching factor, we may investigate averaging the autoionization decay rate $\Gamma(n,\ l)$ from Eq. (7.7) over the orbital quantum number, i.e.,

$$\langle W_A(n,l)\rangle = 1.7\frac{f_{if}Z_i^2}{\pi n^5\omega}. \tag{7.34}$$

For the corresponding total DR rate, we then obtain

$$\langle DR(\text{a.u.})\rangle = \frac{0.86\times10^2}{T_e^{3/2}}\left(\frac{Z_n}{Z_i}\right)^2\int_0^{x_0}dx\; x^2\left[\frac{\varphi(x,q)}{x}\right]^{9/4} \times\int_1^\infty dt\;\frac{\exp\left\{-\dfrac{1.2Z}{T_e}\left[\dfrac{\varphi(x,q)}{x}\right]^{3/4}\left(1-\dfrac{1}{t^2}\right)\right\}}{t^5+A(x)}, \tag{7.35}$$

$$A(x) = \frac{4.56\times10^6}{Z_i^3\sqrt{Z_n}\left[\dfrac{\varphi(x,q)}{x}\right]^{3/8}}.$$

For heavy ions, the quantum mechanical level-by-level calculations are very complex and have so far been carried out mainly for closed-shell configurations. Only recently have open-shell configurations also been considered.[69,70] In open-shell configurations (e.g., the open $4p$, $4d$, and $4f$ shells, or even higher ones such as the $5p$, $5d$, $5f$, and $5g$ shells), excitation–autoionization channels are very complex, and the overall completeness of quantum mechanical level-by-level calculations should still be considered with care. Analysis shows that order-of-magnitude disagreements can be expected at low temperatures, while at high temperatures, different level-by-level quantum mechanical models differ by about a factor of 2, and the Burgess–Mertz approach[32] may deviate by many orders of magnitude and also gives an entirely inadequate temperature dependence, as demonstrated by more detailed calculations.[71]

Below, we compare the different approaches with detailed quantum mechanical level-by-level calculations of the DR rates. Figure 3 shows the total DR rates of xenon Xe^{26+} and gold Au^{51+} (the Ni-like $3s^23p^63d^{10}$ configuration into which dielectronic capture proceeds) calculated with the l-averaged statistical model from Eqs. (7.33)–(7.35) that employs the Thomas–Fermi model of Eqs. (7.19)–(7.31), the

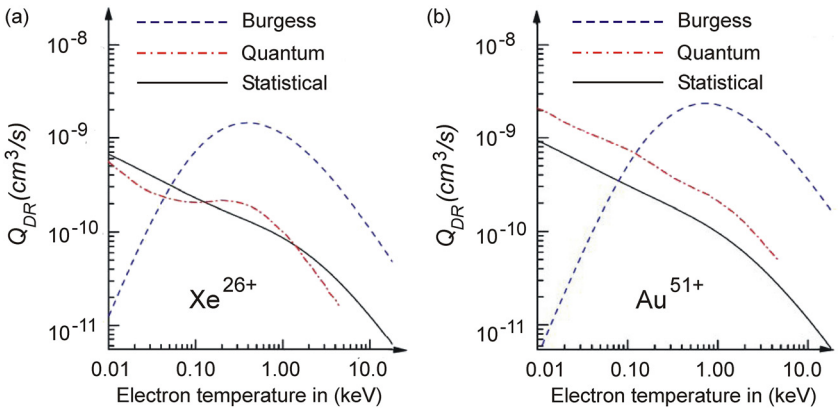

FIG. 3. Comparison of the *l*-averaged statistical approach with the Burgess and quantum level-by-level calculations for the Ni-like sequence $3s^2 3p^6 3d^{10}$ of Xe^{26+} and Au^{51+}.

Burgess–Mertz formula from Eqs. (3.10)–(3.15), and the quantum level-by-level calculations from Ref. 71.

The statistical model compares quite well (within a factor of two) over a very large temperature interval until very low temperatures, while the Burgess approach entirely fails to describe the total DR rate of heavy ions. Similar observations are made for other isoelectronic sequences. Figure 4 shows a comparison of the results from the different approaches for the DR rates of Sr-like ($4s^2 4p^6 4d^2$) and Zn-like ($4s^2$) tungsten W^{36+} and W^{44+}, respectively.[70]

It is particularly impressive that the statistical model provides a rather good approximation of the total DR rate in the low-temperature region that is numerically exceedingly difficult to treat by fully quantum mechanical level-by-level calculations. Thus, the statistical model in its simplest version seems to provide even the possibility of estimating the order-of-magnitude correctness of very complex quantum level-by-level calculations. Moreover, it should be remembered that currently even the most sophisticated quantum level-by-level calculations[70] have been performed only in the low-density limit (the coronal model: a low-density limit in which three-body recombination may be entirely neglected), where the branching factors are entirely determined by radiative and autoionization decay rates while dielectronic capture proceeds from the respective ground states of the various charge states only. In high-density plasmas, however, as discussed above, collisional depopulation is due to electron collisional ionization or collisional transfer to other levels. In addition, excited states are highly populated, and very efficient channels of DR may proceed from these. This may entirely change the properties of the total DR rate, because dielectronic capture into excited states can be even more important than the corresponding capture to the ground state. This effect has been explicitly confirmed by high-resolution X-ray spectroscopy of dense laser-produced plasmas, where it has been shown that DR into excited states can exceed by many orders of magnitude the corresponding DR into ground states.[23,45] For high-*Z* elements and open *M*, *N*, and *O* shells, excited states might be highly populated even at rather moderate electron densities. Therefore, all current detailed quantum level-by-level calculations to determine the DR rate have to be considered with care for each particular application. In this respect, the properties and the innovation potential of the statistical model look very advantageous for the determination of total DR rates for heavy elements.

Finally, it should be noted that the inclusion of more levels in the detailed quantum mechanical level-by-level calculations may not

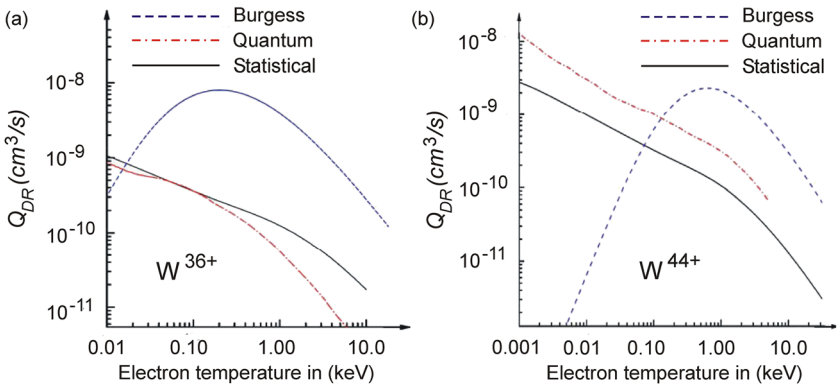

FIG. 4. Comparison of the *l*-averaged statistical approach with the Burgess and quantum level-by-level calculations for the Sr-like sequence $4s^2 4p^6 4d^2$ of W^{36+} and the Zn-like sequence $4s^2$ of tungsten W^{44+}.

necessarily result only in an increase in the DR rate, but can also lead to a decrease, as discussed in Sec. III. Therefore, at present, the simple statistical method as presented above compares quite well with other available much more complex methods of calculation and has the advantages of generality and ease of application. In addition, there is much room for improvement to the statistical model via improvements to the Thomas–Fermi model (ionization energies, l-quantum-number dependence, adopting the Vlasov approach instead of the local plasma frequency etc.).

VIII. CONCLUSION

Dielectronic recombination (DR) can be cast as a product of dielectronic capture and a probability for radiative stabilization of the excited core followed by radiative decay of the spectator electron to the ground state. In the limiting case of negligible collisions compared with radiative decay, the total DR rate is a function of atomic structure constants only; i.e., the DR rate is a function of radiative decays, Auger rates, energy levels, statistical weights, and temperature. The quantum mechanical multichannel coupling (QMMC) approach demonstrates that the Burgess theory (including the Burgess–Mertz formulas) of DR may overestimate higher-order contributions by orders of magnitude. Collisional processes are identified to have multiple impacts on DR: (a) electron collisional excitation drives excited-state couplings that are often even more important than ground-state contributions; (b) angular-momentum-changing collisions between autoionizing states change the effective core relaxation and induce DR rates that are dependent on density—an effect that manifests itself in a perturbation of the spectral distribution of dielectronic satellite spectra; (c) collisional ionization of the spectator electron reduces high-n contributions to DR if ionizations are more frequent than radiative stabilizations of the core and the spectator electron. The plasma microfield strongly influences high-n DR contributions via ionization potential depression and perturbations of the spherical symmetry of autoionization matrix elements. Approximate calculations of DR rates, such as the quasiclassical method and Vainshtein's approximate QMMC approach (which allows treatment of very large quantum numbers without convergence problems) combined with atomic population kinetic effects (excited-state-driven DR, angular-momentum-changing collisions, ionization potential depression, and collisional ionization of the spectator electron before radiative relaxation) are identified as providing effectively higher precision for the total DR rate than pure atomic structure calculations (even though the latter are more sophisticated). Finally, the first steps have been undertaken in a statistical approach to DR that is based on the local plasma frequency approximation rather than on standard atomic structure calculations. Quite good agreement with the most advanced quantum mechanical calculations so far available have been obtained, opening up a new field of activity for the plasma atom approach. Moreover, as DR has an impact on all ionization balance calculations, an accurate treatment of DR is mandatory and therefore remains an active and important field of research in atomic physics. On the other hand, spectroscopic diagnostics based on dielectronic satellite transitions provide a unique characterization of very complex phenomena and therefore contribute considerably to advances in many different areas of atomic and plasma physics.

ACKNOWLEDGMENTS

This work was supported by the Cooperation Agreement between the Sorbonne University (Faculty of Sciences) and the Moscow Institute of Physics and Technology—MIPT. Financial support from MIPT under Grant No. 075-02-2019-967 in the framework of the 5-top-100 program is greatly acknowledged. This work has also been supported by the Competitiveness Program of NRNU MEPhI in the framework of the Russian Academic Excellence Project.

REFERENCES

[1]H. R. Griem, *Principles of Plasma Spectroscopy* (Cambridge University Press, New York, 1997).
[2]F. B. Rosmej, V. A. Astapenko, and V. S. Lisitsa, *Plasma Atomic Physics* (Springer, 2020).
[3]A. Burgess, "Dielectronic recombination and the temperature of the solar corona," Astrophys. J. **139**, 776 (1964); "Dielectronic recombination and the temperature of the solar corona," **141**, 1588 (1965).
[4]A. H. Gabriel, "Dielectronic satellite spectra for highly-charge helium-like ion lines," Mon. Not. R. Astron. Soc. **160**, 99 (1972).
[5]V. A. Vinogradov, I. Yu. Skobelev, and E. A. Yukov, "Effect of collisions on the intensities of the dielectronic satellites of resonance lines of hydrogenlike ions," Sov. Phys. JETP **45**, 925 (1977).
[6]V. L. Jacobs and M. Blaha, "Effects of angular-momentum-changing collisions on dielectronic satellite spectra," Phys. Rev. A **21**, 525 (1980).
[7]F. B. Rosmej and J. Abdallah, Jr., "Blue satellite structure near He_α and He_β and redistribution of level populations," Phys. Lett. A **245**, 548 (1998).
[8]L. A. Woltz, V. L. Jacobs, C. F. Hooper *et al.*, "Effects of electric microfields on argon dielectronic satellite spectra in laser-produced plasmas," Phys. Rev. A **44**, 1281 (1991).
[9]E. Galtier, F. B. Rosmej, A. Calisti *et al.*, "Interference effects and Stark broadening in XUV intra-shell transitions in aluminum under conditions of intense XUV free electron laser irradiation," Phys. Rev. A **87**, 033422 (2013).
[10]F. B. Rosmej, "Hot electron x-ray diagnostics," J. Phys. B: At., Mol. Opt. Phys. **30**, L819 (1997).
[11]S. H. Glenzer, F. B. Rosmej, R. W. Lee *et al.*, "Measurements of suprathermal electrons in hohlraum plasmas with x-ray spectroscopy," Phys. Rev. Lett. **81**, 365 (1998).
[12]M. Smid, O. Renner, A. Colaitis *et al.*, "Characterization of suprathermal electrons inside a laser accelerated plasma via highly-resolved K_α emission," Nat. Commun. **10**, 4212 (2019).
[13]E. Galtier, F. B. Rosmej, D. Riley *et al.*, "Decay of crystaline order and equilibration during solid-to-plasma transition induced by 20-fs microfocused 92 eV free electron laser pulses," Phys. Rev. Lett. **106**, 164801 (2011).
[14]F. B. Rosmej and R. W. Lee, "Hollow ion emission driven by pulsed x-ray radiation fields," Europhys. Lett. **77**, 24001 (2007).
[15]J. Colgan, J. Abdallah, Jr., A. Y. Faenov *et al.*, "Exotic dense-matter states pumped by a relativistic laser plasma in the radiation-dominated regime," Phys. Rev. Lett. **110**, 125001 (2013).
[16]F. B. Rosmej, H. R. Griem, R. C. Elton *et al.*, "Investigation of charge exchange induced formation of two electron satellite transitions in dense laser produced plasmas," Phys. Rev. E **66**, 056402 (2002).
[17]F. B. Rosmej, V. S. Lisitsa, R. Schott *et al.*, "Charge exchange driven X-ray emission from highly ionized plasma jets," Europhys. Lett. **76**, 815 (2006).
[18]F. B. Rosmej and V. S. Lisitsa, "A self-consistent method for the determination of neutral density from X-ray impurity spectra," Phys. Lett. A **244**, 401 (1998).
[19]F. B. Rosmej, D. Reiter, V. S. Lisitsa *et al.*, "Influence of charge exchange processes on X-ray spectra in TEXTOR tokamak plasmas: Experimental and theoretical investigation," Plasma Phys. Controlled Fusion **41**, 191 (1999).
[20]F. B. Rosmej and V. S. Lisitsa, "Non-equilibrium radiative properties in fluctuating plasmas," Plasma Phys. Rep. **37**, 521 (2011).

[21]F. B. Rosmej and A. Y. Faenov, "New innershell phenomena from Rydberg series of highly charged ions," Phys. Scr. **T73**, 106 (1997).
[22]F. B. Rosmej, A. Y. Faenov, T. A. Pikuz *et al.*, "Inner-shell satellite transitions in dense short pulse plasmas," J. Quant. Spectrosc. Radiat. Transfer **58**, 859 (1997).
[23]F. B. Rosmej, A. Y. Faenov, T. A. Pikuz *et al.*, "Line formation of high intensity He_β-Rydberg dielectronic satellites $1s3lnl'$ in laser produced plasmas," J. Phys. B: At., Mol. Opt. Phys. **31**, L921 (1998).
[24]O. Renner, E. Krouský, F. B. Rosmej *et al.*, "Observation of H-like Al Ly_α disappearance in dense cold laser produced plasmas," Appl. Phys. Lett. **79**, 177 (2001).
[25]B. Deschaud, O. Peyrusse, and F. B. Rosmej, "Simulation of XFEL induced fluorescence spectra of hollow ions and studies of dense plasma effects," Phys. Plasmas **27**, 063303 (2020).
[26]I. I. Sobelman and L. A. Vainshtein, *Excitation of Atomic Spectra* (Alpha Science, 2006).
[27]J. G. Rubiano, R. Florido, C. Bowen *et al.*, "Review of the 4th NLTE code comparison workshop," High Energy Density Phys. **3**, 225 (2007).
[28]H.-K. Chung, C. Bowen, C. J. Fontes *et al.*, "Comparison and analysis of collisional-radiative models at the NLTE-7 workshop," High Energy Density Phys. **9**, 645 (2013).
[29]J. Colgan, C. F. Fontes, H. Zhang *et al.*, "Collisional-radiative modeling of tungsten at temperatures of 1200–2400 eV," Atoms **3**, 76 (2015).
[30]A. Sommerfeld, *Atombau und Spektrallinien* (Harri Deutsch, 1978), Vol. II.
[31]V. I. Kogan, A. B. Kukushkin, and V. S. Lisitsa, "Kramers electrodynamics and electron-atomic radiative collisional processes," Phys. Rep. **213**, 1 (1992).
[32]R. D. Cowan, *The Theory of Atomic Structure and Spectra* (California University Press, 1981).
[33]*Handbook of Atomic, Molecular, and Optical Physics*, edited by G. W. F. Drake (Springer, 2006).
[34]A. Pradhan and S. N. Nahar, *Atomic Astrophysics and Spectroscopy* (Cambridge University Press, Cambridge, 2011).
[35]V. A. Astapenko, *Polarization Bremsstrahlung on Atoms, Plasmas, Nanostructures and Solids* (Springer, 2013).
[36]L. A. Vainshtein and U. I. Safronova, "Wavelengths and transition probabilities of satellites to resonance lines of H- and He-like ions," At. Data Nucl. Data Tables **21**, 49 (1978).
[37]F. F. Goryaev, L. A. Vainshtein, and A. M. Urnov, "Atomic data for doubly-excited states $2lnl'$ of He-like and $1s2lnl'$ of Li-like ions with Z=6-36 and n=2,3," At. Data Nucl. Data Tables **113**, 117 (2017).
[38]I. L. Beigman, L. A. Vainshtein, and B. N. Chichkov, "Dielectronic recombination," J. Exp. Theor. Phys. **53**, 490 (1981).
[39]V. S. Lisitsa, *Atoms in Plasmas* (Springer, 1994).
[40]D. S. Leontyev and V. S. Lisitsa, "Statistical model of dielectronic recombination of heavy ions in plasmas," Contrib. Plasma Phys. **56**, 846 (2016).
[41]A. V. Demura, D. S. Leont'iev, V. S. Lisitsa *et al.*, "Statistical dielectronic recombination rates for multielectron ions in plasma," J. Exp. Theor. Phys. **125**, 663 (2017).
[42]V. P. Shevelko and L. A. Vainshtein, *Atomic Physics for Hot Plasmas* (IOP Publishing, Bristol, 1993).
[43]L. A. Vainshtein and V. P. Shevelko, *Program ATOM*, Preprint No. 43, Lebedev Physical Institute, Moscow 1996.
[44]L. A. Vainshtein, Proc. P. N. Lebedev Inst. **119**, 3 (1980).
[45]F. Petitdemange and F. B. Rosmej, "Dielectronic satellites and Auger electron heating: Irradiation of solids by intense XUV-free electron laser radiation," in *New Trends in Atomic & Molecular Physics: Advanced Technological Applications*, edited by M. Mohan (Springer, 2013), Vol. 76, pp. 91–114, ISBN: 978-3-642-38166-9.
[46]F. B. Rosmej, "Diagnostic properties of Be-like and Li-like satellites in dense transient plasmas under the action of highly energetic electrons," J. Quant. Spectrosc. Radiat. Transfer **51**, 319 (1994).
[47]F. B. Rosmej, "A new type of analytical model for complex radiation emission of hollow ions in fusion and laser produced plasmas," Europhys. Lett. **55**, 472 (2001).
[48]F. B. Rosmej, "An alternative method to determine atomic radiation," Europhys. Lett. **76**, 1081 (2006).
[49]F. B. Rosmej, "X-ray emission spectroscopy and diagnostics of non-equilibrium fusion and laser produced plasmas," in *Highly Charged Ion Spectroscopic Research*, edited by Y. Zou and R. Hutton (Taylor and Francis, 2012), pp. 267–341, ISBN: 9781420079043.
[50]X. Li, F. B. Rosmej, V. A. Astapenko *et al.*, "An analytical plasma screening potential based on the self-consistent-field ion-sphere model," Phys. Plasmas **26**, 033301 (2019).
[51]X. Li and F. B. Rosmej, "Analytical approach to level delocalization and line shifts in finite temperature dense plasmas," Phys. Lett. A **384**, 126478 (2020).
[52]H. A. Bethe and E. E. Salpeter, *Quantum Mechanics of One- and Two-Electron Atoms* (Plenum Publishing, New York, 1977); (a) J. D. Hey, "On the role of atomic metastability in the production of Balmer line radiation from cold atomic hydrogen, deuterium and hydrogenic ion impurities in fusion edge plasmas," J. Phys. B: At., Mol. Opt. Phys. **45**, 065701 (2012).
[53]J. Davis and V. L. Jacobs, "Effects of plasma microfields on radiative transitions from atomic levels above the ionization threshold," Phys. Rev. A **12**, 2017 (1975).
[54]V. L. Jacobs, J. Davis, and P. C. Kepple, "Enhancement of dielectronic recombination by plasma electric microfields," Phys. Rev. Lett. **37**, 1390 (1976).
[55]V. L. Jacobs and J. Davis, "Properties of Rydberg autoionizing states in electric field," Phys. Rev. A **19**, 776 (1979).
[56]M. F. Gu, "The flexible atomic code FAC," Can. J. Phys. **86**(5), 675 (2008); (a) I. P. Grant and N. C. Pyper, "Breit interaction in multi-configuration relativistic atomic calculations," J. Phys. B: A., Mol. Phys. **9**, 761 (1976).
[57]L. A. Bureyeva, T. Kato, V. S. Lisitsa *et al.*, "Quasiclassical representation of autoionization decay reates in parabolic coordinates," J. Phys. B: At., Mol. Opt. Phys. **34**, 3909 (2001).
[58]L. A. Bureyeva, T. Kato, V. S. Lisitsa *et al.*, "Quasiclassical theory of dielectronic recombination in plasmas," Phys. Rev. A **65**, 032702 (2002).
[59]F. Robicheaux and M. S. Pindzola, "Enhanced dielectronic recombination in crossed electric and magnetic fields," Phys. Rev. Lett. **79**, 2237 (1997); (a) J. D. Hey, "On the Runge-Lenz-Pauli vector operator as an aid to the calculations of atomic processes in laboratory and astrophysical plasmas," J. Phys. B: At., Mol. Opt. Phys. **48**, 185701 (2015); (b) "On the use of the axially symmetric paraboloidal coordinate system in deriving some properties of Stark states of hydrogenic atomc and ions," J. Phys. A: Math. Theor. **52**, 045203 (2019).
[60]P. Gombas, "Erweiterung der statistischen theroy des atoms," Z. Phys. **121**, 523 (1943).
[61]P. Gombas, *Die statistische theorie des Atoms und ihre Anwendungen* (Springer-Verlag, Wien, 1949).
[62]P. Gombás, "Present state of the statistical theory of atoms," Rev. Mod. Phys. **35**, 512 (1963).
[63]P. Fromy, C. Deutsch, and G. Maynard, "Thomas-Fermi-like and average atom models for dense and hot matter," Phys. Plasmas **3**, 714 (1996).
[64]E. H. Lieb and B. Simon, "The Thomas-Fermi theory of atoms, molecules and solids," Adv. Math. **23**, 22 (1977).
[65]G. Kemister and S. Nordholm, "A radially restricted Thomas-Fermi theory for atoms," J. Chem. Phys. **76**, 5043 (1982).
[66]A. V. Demura, M. B. Kadomtsev, V. S. Lisitsa *et al.*, "Universal statistical approach to radiative and collisional processes with multielectron ions in plasmas," High Energy Density Phys. **15**, 49 (2015).
[67]A. Sommerfeld, "Integrazione asintotica dell'equazione differentiale di Thomas–Fermi," Rend. R. Accad. Lincei **15**, 293 (1932).
[68]V. D. Kirillow, B. A. Trubnikov, and S. A. Trushin, "Role of impurities in anomalous plasma resistance," Sov. J. Plasma Phys. **1**, 117 (1975).
[69]C. P. Balance, S. D. Loch, M. S. Pindzola *et al.*, "Dielectronic recombination of W^{35+}," J. Phys. B: At., Mol. Opt. Phys. **43**, 205201 (2010).
[70]Z. Wu, Y. Fu, X. Ma *et al.*, "Electronic impact excitation and dielectronic recombination of highly charged tungsten ions," Atoms **3**, 474 (2015).
[71]E. Behar, P. Mandelbaum, J. L. Schwob *et al.*, "Dielectronic recombination rate coefficients for highly-ionized Ni-like atoms," Phys. Rev. A **54**, 3070 (1996).